A common European approach to the regulatory testing of nanomaterials

NANoREG

Grant Agreement Number 310584

Deliverable D 3.4

Improved data for the modelling of the exposure to MNMs

Due date of deliverable: *2015-12-31*

Actual submission date: *2015-12-24*

Author(s) and company:	Asmus Meyer-Plath, BAuA; Ismo Koponen, Alexander Jensen, Joonas Koivisto, NRCWE; Emmanuel Belut, INRS; Araceli Sanchez, Martie van Tongeren, Laura MacCalman, IOM; Ilse Tuinman, Wouter Fransman, TNO; Maidá Domat, ITENE; Marija Bivolarova, Jørn Toftum Danish,Technical University.
Work package/task:	WP 3 / Task 3.4
Document status:	draft / final
Confidentiality:	confidential / restricted / public
Key words:	

DOCUMENT HISTORY

Version	*Date*	*Reason of change*
1	2015-12-24	1st submission
2	2016-05-30	2nd submission
3	2017-03-08	Project Office harmonized lay-out
4		

This work is licensed under the Creative Commons Attribution-NonCommercial-ShareAlike 4.0 International License.

To view a copy of this license, visit http://creativecommons.org/licenses/by-nc-sa/4.0/ or send a letter to Creative Commons, PO Box 1866, Mountain View, CA 94042, USA.

This project has received funding from the European Union Seventh Framework Programme (FP7/2007-2013) under grant agreement no 310584

Lead beneficiary for this deliverable:
Bundesanstalt für Arbeitsschutz und Arbeitsmedizin, BAuA, Partner 3

Owner(s) of this document	
Asmus Meyer-Plath	BAuA, Partner 3
Ismo Koponen, Alexander Jensen, Joonas Koivisto	NRCWE, Partner 4
Emmanuel Belut	INRS, Partner 21
Araceli Sanchez, Martie van Tongeren, Laura McCalman	IOM, Partner 9
Ilse Tuinman, Wouter Fransman	TNO, Partner 31
Maidá Domat	ITENE, Partner 42
Marija Bivolarova, Jørn Toftum	Danish Technical University, External partner

Table of Content

1 DESCRIPTION OF TASK 5

2 DESCRIPTION OF WORK & MAIN ACHIEVEMENTS 5

2.1 SUMMARY 5

2.2 BACKGROUND OF THE TASK 6

2.3 REGULATORY QUESTIONS 7

2.4 EXPOSURE MODELS 7

2.5 DESCRIPTION OF THE WORK CARRIED OUT 10

2.5.1 The premises 11

2.5.1.1 Room geometry 11

2.5.1.2 Ventilation system 12

2.5.2 The sources 14

2.5.2.1 Tracer gas injection 14

2.5.2.2 Nanoparticle nebulization 14

2.5.2.3 Oil mist nebulization 15

2.5.2.4 Disc feeding 15

2.5.2.5 Source calibration approaches 15

2.5.2.6 Source operation modes 15

2.5.2.7 Source location 16

2.5.3 The nanomaterials 16

2.5.4 Definition of near and far field volumes 16

2.5.5 The instrumentation 17

2.5.5.1 Nanoparticle monitors 18

2.5.5.2 Surface sampler 19

2.5.5.3 Tracer gas sensing devices 19

2.5.6 Aerosol sampling and instrument positioning 20

2.5.7 Data collection and documentation 24

2.5.7.1 Data formatting and chunking 24

2.5.8 Type of experiments performed 25

2.5.8.1 Age of air 25

2.5.8.2 Tracer gas distribution 25

2.5.8.3 Aerosol sampling 26

2.5.8.4 Surface sampling 26

2.5.9 Experimental schedule 26

2.6 RESULTS 28

2.6.1 Performed preparatory experiments 28

2.6.1.1 Age of air experiments 28

2.6.1.2 Instrument inter-comparison experiments 30

2.6.2 Performed exposure experiments 31

2.6.2.1 Source position variation experiments 31

2.6.2.2 Spiking experiments 34

2.6.2.3 Coagulation experiment 36

2.6.2.4 Deposition Results 37

2.7 DISCUSSION 38

2.7.1 Data quality 38
2.7.2 Identified data gaps 38
2.8 EVALUATION AND CONCLUSIONS 39
2.8.1 Use of data to understand determinants of exposure 39
2.8.2 Use of data to test quantitative exposure models 39
2.8.3 Answers to regulatory questions 40
2.8.4 Provision of data for testing exposure models and assessment tools 40
3 DEVIATIONS FROM THE WORK PLAN 41
4 ANNEX 42

1 Description of task

Exposure modelling is extensively used in regulatory exposure assessment. Such exposure models will need extensive validation and/or calibration in order to improve accuracy of the tools and to develop new modelling approaches or tools.

A framework for modelling of inhalation exposure to nanoparticles has been proposed by Schneider et al. (2011) which has been used as a basis for the development of a number of existing tools, e.g. NANOSAFER, STOFFENMANAGER-NANO and the 2-box model developed by IOM. Exposure models can be semi-quantitative and used as the basis for the selection of controls (control banding approach) (e.g. NANOSAFER, STOFFENMANAGER-NANO) although models could also be developed that provide quantitative exposure estimates. The aim of task 3.4 of the NANOREG project was

a. To evaluate and compare existing exposure models using data already collected as well as data collected as part of this project

b. If necessary, to modify and adapt existing models and develop new models

c. Re-evaluate and promulgate these new models.

2 Description of work & main achievements

2.1 Summary

A comprehensively-monitored nanoparticle exposure experiment inside a large climate-controlled chamber at Danish Technical University was conducted as a joint experiment in the frame of the task 3.4 of the NANoREG project. Experimental data on spatial and temporal distributions of MNM have been collected with high resolution under controlled conditions, varying emission patterns, ventilation rates and particle composition.

The data were used to test the quantitative exposure models and to estimate the accuracy and uncertainty of the predicted concentrations. The accuracy can be evaluated for different exposure scenarios, including stationary and transient spiking emission as well as bimodal coagulation conditions. The level of control and understanding of these experimental scenarios was studied by means of advanced 3D-CFD (computational fluid dynamics) simulations that allow extrapolation of experimental sampling data in time, space and particle size distribution.

As a result, after matching experimental and CFD data, the results of this experiment helped to provide key information for addressing questions 11 and 12 from the regulatory questions of the project through:

- Characterization of the emitted particles in terms of airborne concentration, size, and morphology at the emission point (time resolved studies) in order to compare and develop accurate exposure models (Q11),
- Investigation of spatial particle characteristics to gain understanding about the transport and fate of particles (Q11),
- Comprehensively reviewing the performance of measuring instruments based on different physical principles and the strengths and weakness for such broad particle characterization experiments (Q11),
- Quantification of required mitigation measures for the potential exposure relative to the task (Q12).

The consortium will make the data publicly available after analysis. This way, a validated dataset will become accessible to external partners who assess exposure models and banding tools.

2.2 Background of the task

The NANoREG project aims to “test the tests”, i.e., evaluating tests and techniques that were developed to understand and assess their health and environmental risk potential of manufactured nanomaterials (MNM).

Since risk assessment requires determination of both exposure dose and toxicity of a substance or material, the techniques of relevance to NANoREG include methods for identifying, characterising, quantifying and toxicological assessment of nanoparticles. All relevant methods were subjected to rigorous testing, with the aim of validating techniques.

Task 3.4 contributed to this goal by focusing on tools for predicting or assessing the exposure to airborne nanoparticles by exposure modelling or control banding. To provide a scientific foundation for the validation of such exposure tools, task 3.4 generated improved data for the modelling of the exposure to MNMs. This was achieved by a joint effort of NANoREG partners as well as external partners to set up, conduct, evaluate and model a series of comprehensively-monitored MNM exposure experiments under temperature and climate-controlled conditions using calibrated MNM emission sources. The work was interlinked with other NANoREG task groups and included their expertise, reference materials and experimental equipment. However, it would not have been possible without the commitment of external partners (DTU, TNO).

Experimental data on spatial and temporal distribution of MNM-containing aerosols were collected with high resolution in a dedicated large-volume climate chamber under controlled conditions. Different exposure scenarios were studied, including stationary, transient spiking and bimodal coagulation conditions.

Evaluation of the exposure situations that were set up and studied experimentally in the frame of task 3.4 were accompanied by computer fluid-dynamic (CFD) modelling. The aim was to obtain a complete description of the exposure scenarios by matching the model and the experimental data. CFD-based reconstruction of the airflow and aerosol dynamics inside of the chamber allowed bridging of the experimental data gaps and led to a more comprehensive data set on the temporal development of aerosol concentrations at virtually every location of the chamber volume. Volume-integrated concentrations were related to the known source strengths and used to test the predictions of simplified exposure tools.

This deliverable report describes the design of the experiment and the results of the measurements. The comparison between measurements and model estimates will be described in Deliverable 3.8.

The data will be made available to external partners for further evaluation. This way, a validated dataset will become available for assessing the different exposure models and assessment tools.

2.3 Regulatory questions

Task 3.4 is concerned with exposure modelling, evaluating models and tools developed to estimate exposure to MNMs with the aim of providing guidance to users and recommendations to developers.

The work carried out by Task 3.4 contributed to providing evidence for two of the NANoREG regulatory questions :

- Question 11: What are the main determinants for occupational and consumer exposure to MNM and what are the duration and type of exposure?
    - Question 11 aims at identifying what the main determinants are, such as
        - material characteristics such as quantities, phase, matrix, and dustiness;
        - process characteristics such as type, confinement, ventilation, duration;
        - worker and consumer characteristics such as tasks and activities.
- Question 12: Exposure: How should human and environmental exposure be assessed in practice (determining exposure scenario, quantify input parameters for models, assumptions and use of proxy indicators, back-ground and uncertainty estimation)?

Having information on determinants of exposure, and how these factors impact on exposure will allow for better, more reliable exposure and hence risk assessments.

Question 12 is concerned with how human and environmental exposure assessment should be carried out. Exposure models play a critical role in exposure assessment. Exposure models can be used to give a first tier estimate of exposure (screening/control banding), while more advanced quantitative models can be used in combination with results from release or concentration measurements to estimate personal exposure levels, or predict exposure in future exposure scenarios. In addition to the development and validation of the models, it is important to provide guidance on how these tools can and should be used in carrying out exposure assessment as part of a wider risk assessment.

2.4 Exposure models

As models and tools are being increasingly used in the exposure (and hazard) assessment of MNMs it is important to understand the uncertainty associated with the tools in order to be able to interpret the results. A thorough evaluation of the tools requires good quality data from experimental as well as field studies.

Evaluation of these tools and models can follow a number of routes depending on the type of model and the output obtained. As the output of the qualitative/semi-quantitative tools is generally a category of exposure (e.g. low, medium, high), measured data may not be necessary, although the ranking of different exposure scenarios can be compared to the relative ranking of exposure measurements associated with them.

Relevant questions that can be investigated include:

- Is the exposure ranking of scenarios the same, or similar, when using tools/models compared to exposure measurement data?
  - If not why not?
- Are there certain circumstances under which the tools perform better, or worse?

Quantitative exposure models can range from complex models that aim to describe the concentrations over space and time with high resolution (such as Computational Fluid Dynamics, CFD, models) and more simple models with reduced resolution over space and/or time.

An example of the latter is a two-box model, where the room or workspace is assumed to consist of two boxes a near-field (NF) (a box either around the worker or the source of emission) and the far-field (FF) (the rest of the room).

This model then estimates the particle number concentration over time in both the NF and the FF, based on

- The location of the source (near or far field) in case the near field is defined as the volume around the worker.
- the emission rate,
- a specified rate of particle flow between the two boxes
- the ventilation rate, which controls the rate at which particles are removed from the room.

Other factors that may be accounted for within the models include:

- losses through deposition on walls, floors and other surfaces
- agglomeration (where the size-resolved concentrations are predicted)
- capture of particles by local controls
- use of other RMMs (e.g. personal protective equipment)

The CFD model in addition to the above factors, also accounts for air flows in order to estimate the concentrations at a large number of points within the room.

Table 1 outlines the inputs required by the two-box and CFD models and their outputs.

Table 1: Inputs required to run the CFD model and the two-box model. The table also shows the outputs that can be obtained from both.

Inputs / Outputs	Two-Box Model	CFD Model
Room	◦ Room dimensions / ◦ Room volume ◦ Surface area of objects in the room	◦ Detailed drawing of the room and all objects/surfaces in it ◦ Position of all inlets, exhausts and all particle sources ◦ Position and shape of thermal loads (heaters, windows, doors)
Ventilation / Air flows	General ventilation rate in the room	For each in/out supply: Mean flow rate Energy rates Velocity distribution Aerosol properties ◦ Mean number concentration ◦ particles mean diameter & GSD ◦ particle size distribution ◦ elemental density of particles ◦ particle morphology
Emission Sources	Emission Rate in Particles/s Particles mean diameter and GSD Time pattern of emission	For each source ◦ source emission rate in particles/s ◦ particles mean diameter & GSD ◦ particle size distribution ◦ elemental density of particles ◦ particle morphology ◦ carrier gas flow rate ◦ emission velocity with direction time pattern of emission
Other Information	Presence of Local controls	
Outputs	Size-resolved particle number concentration in the two boxes over time	◦ mean air velocity field in the room ; ◦ mean pressure field in the room ; ◦ fields of turbulent kinetic energy and its dissipation rate throughout the room ; ◦ mean temperature field in the room (for non-isothermal cases) ; ◦ fields of the mean 6 first moments of the particle size distribution of the aerosol in the room and at each outlet/exhaust ; ◦ fields of the deposition flux of the 6 first moments of the PSD at walls ; ◦ time variations of the above if the case is transient/unsteady.

Although data collected during small-scale experiments and field studies have been used to test the models to date, it is clear that to ensure the models are reliable in predicting real world concentrations, or at the very least to identify the uncertainty related to the predicted concentrations, further data need to be collected for model validation. The large-scale experiment described below was designed specifically to collect data to test the quantitative exposure models. The input parameters for the models are known (i.e. emission rate, ventilation rate, dimensions of room, position of source, position of ventilation, position of equipment) and the concentrations throughout the room were measured, using a variety of measurement equipment, over time. These data will be used to compare the predictions with measurement results, which will be described in Deliverable 3.8.. Such comparisons will enable guidance to be developed on when and how to use these models and how reliable their predictions are likely to be.

2.5 Description of the work carried out

The data and analysis presented in this report were collected during a joint experiment organised by Task 3.4 in the frame of the project NANoREG. It aimed at providing a comprehensive data set for the modelling of the exposure to MNMs.

Due to the complexity of aerosol dynamics, a large-volume of particle-free-air supplied chamber with temperature and humidity control was selected as the experimental environment. To disturb the airflow inside as little as possible, nanoparticle monitors were placed outside of the chamber. They sampled the aerosol using sampling gas lances, for which the particle loss probability was calculated. In order to study the temporal development of the aerosol concentration and size distribution with as much detail as possible, a large number of aerosol monitors was put to operation by a joint effort of NANOREG partners as well as external collaborators. To map the airflow, tracer gases were added to the emission source and monitored by laser absorption spectroscopy.

A series of different release scenarios was conducted using source strength-calibrated nanoparticle emitters. Prior to the experiments, inter-comparison experiments of the monitoring instruments were performed.

After completion of the experiments the data were collected, collated and checked for consistency. First analyses of the experimental data provide valuable insight into the chamber airflow dynamics at different sampling locations.

The following section describes experimental details of the work performed.

2.5.1 *The premises*

The experiments were performed within a climate chamber ("Chamber 7") at the Department of Civil Engineering at Danish Technical University (DTU) in Copenhagen. The climate chamber allowed full control of air exchange rates, temperature and humidity. The chamber was positioned inside a large hall, granting full access to all chamber walls, floor and ceiling (Figure 1).

2.5.1.1 *Room geometry*

By means of modular, lifetable ceiling element frame, a movable inner wall, the height and size as well as the in- and outlets of "Chamber 7" were adapted to the requirements of the experiment. The chamber volume was maximised to L x W x H = 6.45 x 4.72 x 2.65 m³ = 80.68 m³ (Figure 2). The air supply inlets and the outlets are also shown in Figure 2. The chamber was sealed by elastomer sealings at the door. All exchangeable elements were sealed by self-adhesive tape (Figure 3).

On top of the chamber, above the ceiling elements, a robust roof frame was installed that allowed to access the roof and to place heavy measurement equipment there (Figure 11). This enabled the partners to keep the measurement equipment out of the chamber, which not only facilitated supervision of the instruments and computers but also ensured that the chamber itself was free of airflow-affecting obstacles.

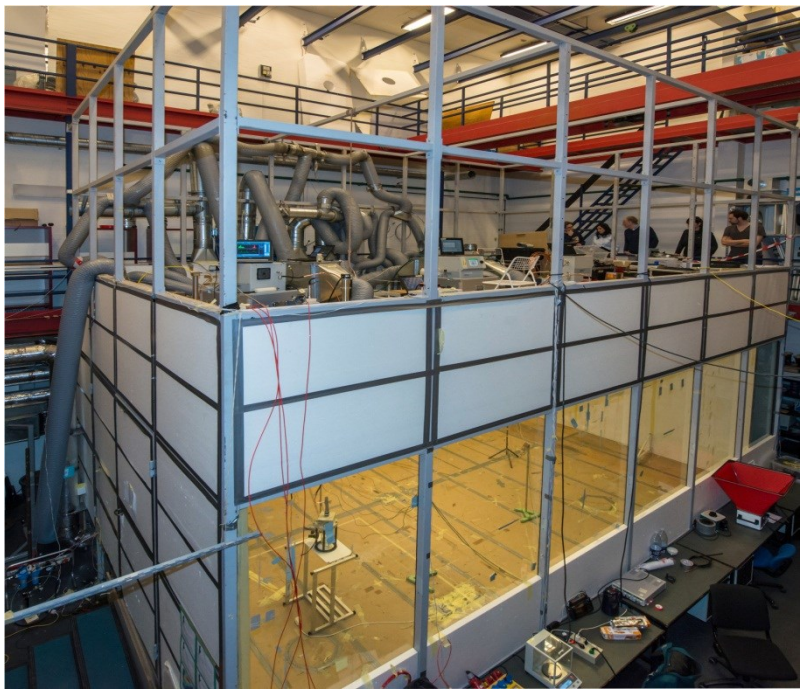

Figure 1: Photo of the DTU climate chamber "7" inside the hall with ventilation and aerosol monitoring installations on the roof.

2.5.1.2 *Ventilation system*

Filtered air (HEPA 14) was supplied to the room by two Lindab PKA 315 diffusers mounted as three-way supplies by means of a triangular deflector (Figure 3), and located as shown on Figure 2. Each supplied up to 400 m³/h. Shutters upstream allowed closing the diffusers. Air was exhausted by a single exhaust located in-between the inlets (Figure 2), also equipped with a Lindab PKA 315 diffuser in omnidirectional configuration.

Table 2: Ventilation conditions used for the experiments.

Target room air exchange Rate Volume/h (V = 78.5 m^3)	Total flow rate Q (exhaust) m³/h	Flow rate for each supply m³/h	Perfect mixing time constant V/Q	Expected flushing time (5 time constants)
0	0	0	∞	∞
3.5	275±5 %	138±5 %	17 min	1 h 25 min
10	786±5 %	393±5 %	6 min	30 min

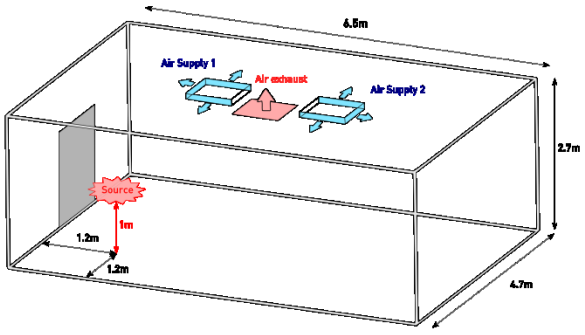

Figure 2: Ventilation configuration of the room.

Figure 3: Lindab PKA315 diffuser with deflector on air supply 2.

Each supply and exhaust was controlled by a separate ventilation system equipped with an orifice plate. Flow-rate calibration for each ventilation system was done separately in the room using a Swema Flow 125 Balometer.

The supplied air was equally distributed between both supplies, and 3 ventilation configurations were considered in the experiments (Table 2). For the specified flow rates, the air velocity profiles around the diffusers were measured with high spatial resolution in a separate setup at INRS, France, using a Kaijo ultrasonic anemometer (Figure 4). Resulting mean velocity vectors in the experimental configuration are shown on Figure 5, for an airflow of 138 m^3/h per diffuser, corresponding to 3.5 air changes per hour (ACH) for a chamber of about 80 m³ equipped with two of these diffusers.

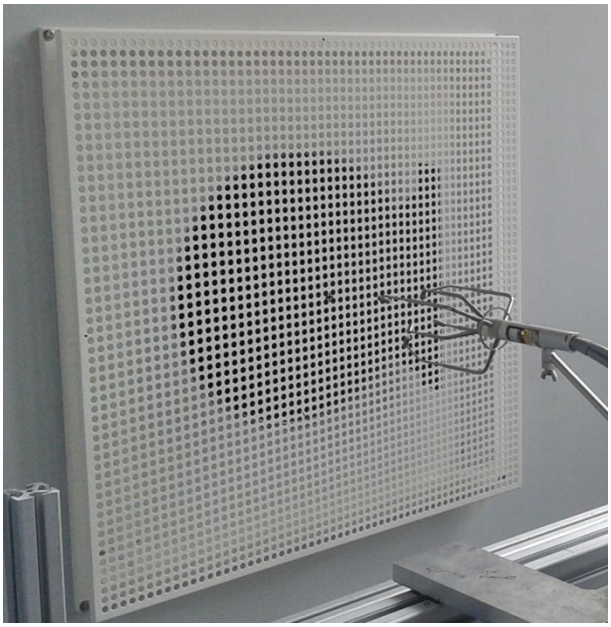

Figure 4: Velocity profile measurements around a PKA315 diffuser.

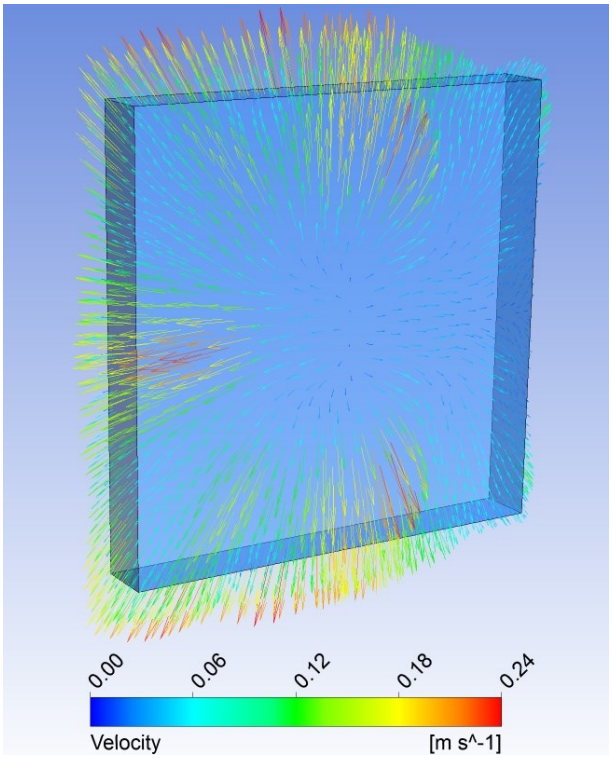

Figure 5: Mean velocity vectors around the diffuser at 138 m^3/h.

2.5.2 *The sources*

2.5.2.1 *Tracer gas injection*

Tracer gases were used in the experiment for two purposes: to characterize the air renewal rate at several points in the room, and to investigate a possible difference of behaviour between airborne nanoparticles and passive gases.

Two types of gases were used in the experiment.

- Ethanol vapours were used as tracer to characterize the air renewal rate in the room. They were generated by means of a PALAS AGF 10 nebulizer fed with liquid ethanol at 90 % and 40 l/min of air. Ethanol vapours were injected upstream of the terminal filters of the two room air inlets, the purpose being to fill the room uniformly with a constant concentration of vapours, before monitoring the time & space dependent decay of vapour concentration in the room. The flow rate of tracer vapours was equally split in two by means of a T-junction, using the same pipe length. The feeding system is shown on Figure 6.
- Tracer gas nitrous oxide (N_2O) was used to study the difference in the behaviour between airborne nanoparticles and passive gases. The N_2O gas was continuously dosed into the nanoparticle generation system through a nylon tube of 3 mm inner diameter. This way the N_2O gas was mixed with the carrier air flow of the nanoparticles. The tracer gas concentration was dosed and sampled using an Innova 1303 doser/sampler system connected to an Innova 1312 photo-acoustic gas analyser. The N_2O feeding rate was 77 mg/s.

Figure 6 : Ethanol vapours injection device for Age of Air measurements.

2.5.2.2 *Nanoparticle nebulization*

The main nanoparticle generation system consisted of a PALAS AGK 2000 nebulizer, fed by a solution of a pure salt in distilled water (see 2.5.3). This nebulizer generated dry crystals of salts by spray-drying of micro-sized droplets. The carrier air flow rate was regulated by means of a Bronkhorst EL-Flow 50 slm mass flow controller, the set-point being digitally given by a laptop, which allowed giving either constant or programmable (time-varying) set-points. Ultra-filtered compressed air was used to feed the nebulizer. The whole setup is depicted in **Error! Reference source not found.**.

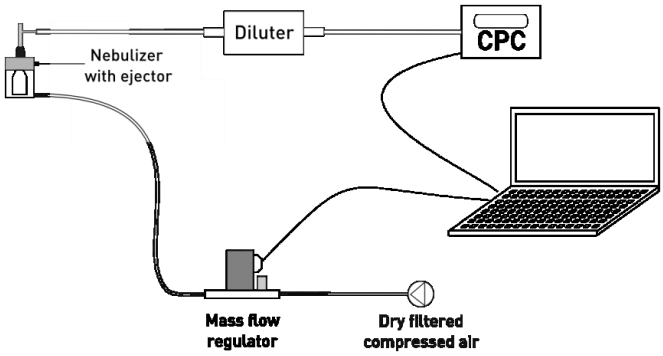

Figure 7: Nanoparticles generation system through nebulization.

Figure 8: Oil mist source PALAS AGF 10.

2.5.2.3 *Oil mist nebulization*

The nebulizer system used for oil mist generation was a PALAS AGF 10 nebulizer (see **Error! Reference source not found.**). Operated at 10 slm air flow, oil mist was injected ownstream of the terminal filters of the two room air inlets.

2.5.2.4 *Disc feeding*

Silica powder of type NM-203 was dispersed using a dry powder aerosol generator (Microdosing system, Fraunhofer ITEM, Hannover, Germany). The generator was operated at a pressure of 1.0 bar which generated airflow of 14.7 L/min.

2.5.2.5 *Source calibration approaches*

When the PALAS AGK 2000 nebulizer was used, i.e., for either NaCl or Na-Fluorescein nanoparticles, the source was calibrated and monitored as follows.

The tip of the nebulizer was equipped with an ejector providing a side sampling junction. 0.3 slm over the 10 slm of the emitted aerosol were sampled and directed towards a PALAS VKL 100 diluter. The diluter provided a 91±3 % dilution factor. The diluted sample was then directed to the GRIM 5403 CNC referred as CPC8 in the experiment, which thus monitored the source continuously. The particle size distribution of the source could also be measured on demand by means of the SMPS (TSI 3081+3082+3088) referred as SMPS1 in the experiment. As the total particle number concentration at the source was stable over time for a given set-point of the mass flow controller, the particle size distribution at the source was not constantly measured. Experience shows that identical saline solution and mass flow of air lead to the same average particle size distribution.

2.5.2.6 *Source operation modes*

- Continuous
  In continuous mode, in order to achieve steady-state aerosol concentration fields in the room, the PALAS AGK 2000 nebulizer was fed by 10 slm of air, with a mass concentration of 0.1 % of salt (either NaCl or Na-Fluorescein).
- Spiking
  For unsteady / spiking sources experiments, the PALAS AGK 2000 nebulizer was fed intermittently by 10 slm of air, with a mass concentration of 0.1 % of salt (NaCl or Na-Fluorescein). The mass flow regulator which controlled the aerosol flow rate followed a time-varying set-point programmed in the laptop, corresponding to window functions (i.e. on/off), following a programmed schedule.
- Twin source operation for MNM emission and tracer gas injection
- Twin source operation for coagulation studies
  For the twin source experiments, the PALAS AGF 10 nebulizer was used with pure olive oil. Olive oil was nebulized into the chamber until the concentration of the oil droplets was stable, acting as a background concentration for the silica NM-203 that was dispersed with the Fraunhofer microdosing system.

2.5.2.7 *Source location*

For all but one experiment, the source was placed at the same location 1.2 m from the front wall and 1.2 m from the left wall of the chamber (see Figure 12). For the coagulation studies, a second nebulizer was operated on the roof of the chamber to inject oil mist into the inlet air. In the same way, also ethanol tracer gas was injected into the inlet air, whereas N_2O was injected into the source carrier gas.

2.5.3 *The nanomaterials*

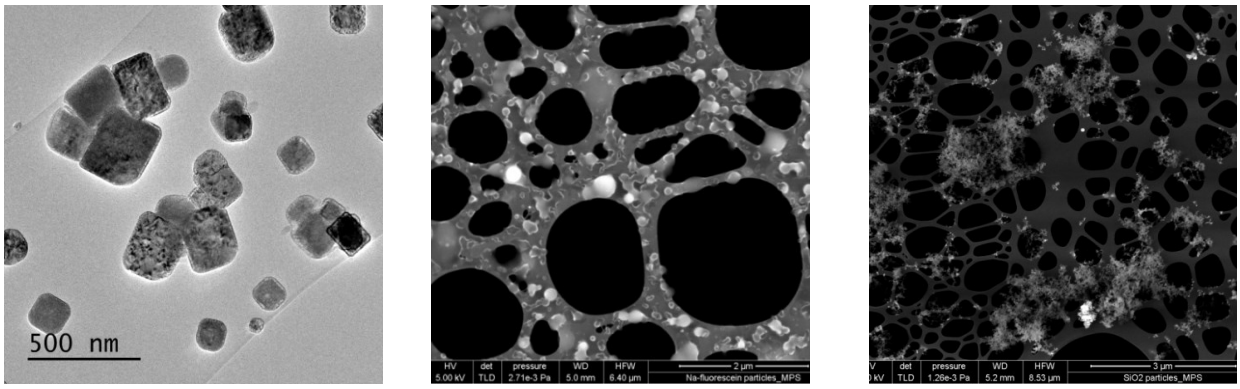

Figure 9: TEM images of the generated NaCl particles (left), Na-fluorescein (middle) and SiO_2 on holey carbon (right).

- NaCl
  The most commonly used nanomaterial in the frame of DTU joint experiment consisted of NaCl crystals generated by spray drying, using the PALAS AGK 2000 nebulizer. These crystals of density 2170 kg/m³ consisted of monomers or aggregates of cubic monomers, as can be seen on Figure 9 (NaCl emitted by a PALAS AGK 2000 and collected on holey grids for transmission electron microscopy - TEM).

- Na-Fluorescein
  Disodium fluorescein (CAS 518-47-8) from Sigma Aldrich was generated by spray drying, with the PALAS AGK 2000 nebulizer in the same way the NaCl was generated. The resulting particles are amorphous spherical particles of density 1602 kg/m³ and consist mainly of monomers and duplicates, as can be seen in Figure 9. This chemical exhibits strong fluorescent properties, which enable its quantitative analysis at very low concentrations.

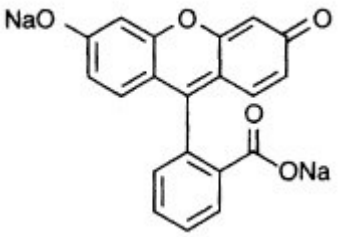

Figure 10: Structure of Na fluorescein.

- SiO_2
  Silica powder of type NM-201 was used. A data sheet can be found in the annex.

- Olive oil
  The mean oil droplet size was about 250 nm (Figure 24).

2.5.4 *Definition of near and far field volumes*

Throughout the experiments, aerosol concentrations and size distributions were measured simultaneously at eight different locations inside of the chamber (Table 3). The term NF has been defined by some as the a volume of 2x2x2 m³ around the emission source. Exposure is then assessed by attributing different average aerosol concentrations to the near and the far

field and by then integrating the residence time of the worker in the two zones. The IOM two-box model aims at estimating the concentrations of the near and far field. Others have defined the NF as the volume of air around the worker (Tielemans et al., 2008)[1]. In this case the exposure of a worker is determined by contributions from sources that are placed in the near field and in the far field.

In this experiment the NF has been defined as the volume of air around the source. During the experiment multiple FF measurements were carried out to study the variability of the far field concentration.

Table 3: Instruments position code and details

Code	IN	SRC	NF	FF1	FF2	SC2	EXH	FF3	FF4
Name	Inlet	Source 1	Near field	Far field 1	Far field 2	Source 2	Exhaust	Far field 3	Far field 4
Location	Directly down-stream of the left inlet air filter	Directly above the source nozzle	0.5 m away in x and y from the source	Opposite of the source w.r.t. the long room axis	At the room centre	Below the exhaust	Inside of the exhaust line	In the corner opposite of the source	Opposite of the source w.r.t. the short room axis

2.5.5 *The instrumentation*

Two kinds of instruments were used, i) real-time devices, which provide specific particle or gas characteristic at the time of the event, and ii) filter samples, which require further off-line analysis. List of instruments and their locations during the experiments is given in

[1] Tielemans E, Schneider T, Goede H, Tischer M, Warren N, Kromhout H, van Tongeren M, van Hemmen J, Cherrie JW Conceptual model for assessment of inhalation exposure: Defining of modifying factors. Annals of Occupational Hygiene doi 10.1093/annhyg/men059 (2008).

Table 4: Instruments used with location, type, serial number, owner, gas flow and residence time in a 2.60 m long gas lance of the specified tube inner diameter. CPC1 moved to a new location at the specified time. The OPC was only operated from Thursday on for oil mist experiments.

. In the following sections, the operating principles and characteristics of the measuring devices will be described briefly.

2.5.5.1 *Nanoparticle monitors*

The mobility particle size distributions were measured with different classes of instruments. They all use particle detection principles based upon electrical mobility of approximately spherical particles, thus variability in measurement accuracy in relation to non-spherical particles is stated by ISO 15900:2009.

- The first class of instrument was a Fast Mobility Particle Sizers (FMPS; Model 3091, TSI Inc., Shoreview, NM, USA) with measurement range from 5.6 to 560 nm. The data are recorded with one second time resolution, thus allowing tracking rapidly changing size distributions. Four FMPSs were available during the experiments
- The second class of instrument was a Scanning Mobility Particle Sizer (SMPS). Two different models were used. Next to the source, Model 3082 from TSI Inc., Shoreview, NM, USA with - in this study - a measurement range from 8.2 nm to 310 nm and one 1 minute time resolution. The SMPS was equipped with a long DMA (Differential Mobility Analyser; Model 3081, TSI Inc., Shoreview, NM, USA) for size classification, a Condensation Particle Counter (CPC, Model 3772, TSI Inc., Shoreview, NM, USA) was used for particle counting and an X-ray Ray Aerosol Neutralizer (Model 3088, TSI Advanced Aerosol Neutralizers, TSI Inc., Shoreview, NM, USA) for neutralizing the charge of particles. The other SMPS instrument was a Grimm 5.403 with long DMA measuring a mobility size range from 10.3 nm to 1094 nm at seven 7 minutes time resolution (GRIMM Aerosol Technik GmbH & Co. KG, Ainring, Germany).
- Thirdly, particle number size distribution spectra were measured using two Electrical Low Pressure Impactors (ELPI+, Dekati Ltd., Finland) which measured the aerodynamic equivalent diameter in 14 channels ranging from 6 nm to 10 µm at 1 s time resolution. Particles are collected on filters that can be further analysed gravimetrically or chemically. Low pressure impactors such as ELPI can report a difference in the particle size distribution due to the de-agglomeration of particles with increased pressure drop when crossing an orifice.

Seven handheld condensation particle counters (CPC) of type TSI 3007 were available. The CPC 3007 can count concentration of particles within a size in range of 10 nm to greater than 1.0 µm in a concentration range of 0 to 100,000 particles/cm³. It uses an optical particle counter; when particles are too small to scatter light and be detected (<300nm), they are grown to larger sizes by condensation of an alcohol. The CPCs operate at an inlet flow of 0.7 slm and has a time resolution of 1 s. A CPC does not classify particles on size or chemical composition.

A nanoparticle surface area monitor (NSAM) 3550 by TSI Inc. measured the human lung-deposited surface area of particles (reported as µm²/cm³) corresponding to tracheobronchial and alveolar regions of the lung. It allows measuring the surface area equivalent dose in the lung. It was operated at an inlet flow of 2.5 slm and reached a time resolution of 1 s.

It complemented a personal nanoparticle monitor of type DiSCmini, which was developed by the University of Applied Sciences and Arts Northwestern Switzerland (FHNW) and is commercially available from Testo AG. The instrument uses the diffusivity properties of corona-charged particles to provide an estimate of particle number concentration, mean diameter and the lung-deposited surface area (LDSA) of a nanoparticle-containing aerosol at 1 s time resolution and complemented too an Optical Particle Sizer (OPS, Model 3330, TSI Inc., Shoreview, NM, USA), based on light scattering equivalent diameter that measures

number and size concentration of particles within a diameter range of 300 nm to 10 µm and a 1 s time resolution.

2.5.5.2 *Surface sampler*

Since real-time devices do not usually distinguish chemical characteristics of the particles, sampling is necessary to identify the chemical composition and shape of the elements present.

Sampling of surface deposition was performed on two types of surface:

1. Electrically conductive carbon tabs (sticky carbon tabs, Agar scientific) for immobilizing samples for scanning electron microscopy
2. Non-conductive polycarbonate membrane filter

Both types of sampling materials were flat circles of 2.5 cm in diameter and were mounted on aluminium pin stubs. The stubs were fastened in a plastic holder, specifically designed to store such samples. These lightweight holders can easily be placed and removed in horizontal and vertical positions e.g. for collecting wall deposition samples. To minimize electrostatic effects, the samples should have been mounted on a grounded metal holder instead of a plastic one.

2.5.5.3 *Tracer gas sensing devices*

The two most important roles of ventilation consist in supplying fresh air for the occupants and to remove airborne pollution, or shortening its residence time as much as possible. The use of tracer gases allows characterizing the ventilation efficiency of a room with respect to these two aspects. It firstly makes it possible to measure the distribution of supplied air in the room, thus assessing the air change effectiveness. It secondly also allows measuring directly the attenuation of pollution by ventilation. Depending on the kind of information which is searched for, the tracing gas is either injected in the ventilation system or as close as possible to the pollution source.

In the present joint experiment, tracer gases were used for these two purposes, firstly to evaluate the air change effectiveness at several location in the room, and secondly to compare the efficiency of ventilation in removing a gas or an aerosol of nanoparticles, so as to highlight a possible specific behaviour of airborne nanoparticles.

Evaluating the air change effectiveness at several locations in the room is useful to evaluate the quality of CFD simulations of airflows in the room.

The two types of tracer gases used were presented beforehand. Each was associated to specific sensors:

- PID – Photo ionization detectors
  Ethanol vapours were used to perform age of air measurements in the room. Ethanol concentrations were measured by means of 12 Alphasense Photo ionization detectors – PID-AH. The sensors were grounded and supplied in energy thanks to a stabilized lab DC power supply. Data were recorded by means of a Graphtec midi logger GL820. As only the time dependency of the concentration decay was needed to compute age of air, the sensors did not require a particular calibration for the experiment, provided that their response varied linearly with concentration.
- Photoacoustic
  The N_2O tracer gas concentration inside of the chamber was quantified using an Innova 1312 Photo-acoustic gas analyser which was attached to an Innova 1303 multipoint samplers, allowing multiple sampling tubes to be measured. The sampling time was set to be 38 s/channel and 6 channels were measured consecutive, resulting in a time resolution of the 6 sampling locations of approximately 4 min. The Innova gas analyser 1312 was calibrated prior to the experiment and its lower detection limit for N_2O gas was 0.05 ppm.

2.5.6 *Aerosol sampling and instrument positioning*

In order to affect the airflow inside of the chamber as little as possible, the stationary online instruments were placed on top of the chamber, see Figure 11. The aerosol sampling was done by connecting the instrument inlets to copper tubes of the same length of 2.60 m. The copper tubes served as gas lances and sampled the aerosol at specified locations of the chamber (Figure 12). Both, the source orifice and the aerosol sampling height of the gas lances were chosen to be 1.20 m, i.e. “about nose height”. The inner diameter of the copper lances was selected according to the aerosol volume intake rate: FMPS and ELPi devices with 10 slm flow rate were connected to tubes of 8 mm inner diameter, whereas CPC, SMPS, DiSCmini and NSAM were connected to tubes of 4 mm inner diameter, see

Table 4: Instruments used with location, type, serial number, owner, gas flow and residence time in a 2.60 m long gas lance of the specified tube inner diameter. CPC1 moved to a new location at the specified time. The OPC was only operated from Thursday on for oil mist experiments.

for further flow rate details of the devices and the calculated residence time of the aerosol in the respective copper tube. The latter shows that the delay time introduced by the aerosol lances is always below 7 s. The lances lead to aerosol particle losses inside of the tube that need to be considered and corrected for(Table 5).

For straight vertical pipes, neglecting electrostatic deposition, particle losses for a given length L can be computed from:

$$C_{out} = C_{in} e^{-\frac{4u^* U_d^+}{Ud} L} \quad (1)$$

where C_{in} and C_{out} are respectively the pipe incoming and outgoing number concentrations, L the pipe length, U the mean flow velocity in the sampling tube, d the pipe diameter, u* the friction velocity in the pipe and U_d^+ the deposition velocity of the particles, which can be given by Eq. (2) according to Wood (1989) :

$$U_d^+ = 0.057 \cdot S_C^{-2/3} + 4.5 \cdot 10^{-4} \cdot \tau^{+2} \quad (2)$$

where $\tau^+ = \frac{\tau u^*}{\nu_f}$ (non-dimensional relaxation time), $S_C = \frac{\upsilon_f}{D_B}$ (Brownian Schmidt Number), and where τ is the particle relaxation time, ν_f is the cinematic viscosity, D_B is the particles Brownian diffusivity. The friction velocity in the pipe can be deduced from the head losses using a correlation for smooth pipes, i.e.$u^* = U\sqrt{\frac{\lambda}{8}}$ where λ is the friction factor. The pipe losses obtained with this relationship for the various lances are given in Table 5, for 3 different particle diameters in the tested range. The percentage of losses for the whole particle size distribution (assuming a PSD identical to that of the NaCl source) is also given. We can observe that pipe losses introduce a measurement bias of only 2%, on average (maximum of 4%).

The sampling pipes also present some bends which increase deposition by centrifugal forces, which will be noticeable for the most inertial particles. Estimating theoretically the corresponding losses is not straightforward and is not done here but should be considered in the future.

Figure 11: Roof of the chamber equipped with ventilation and measurement instruments.

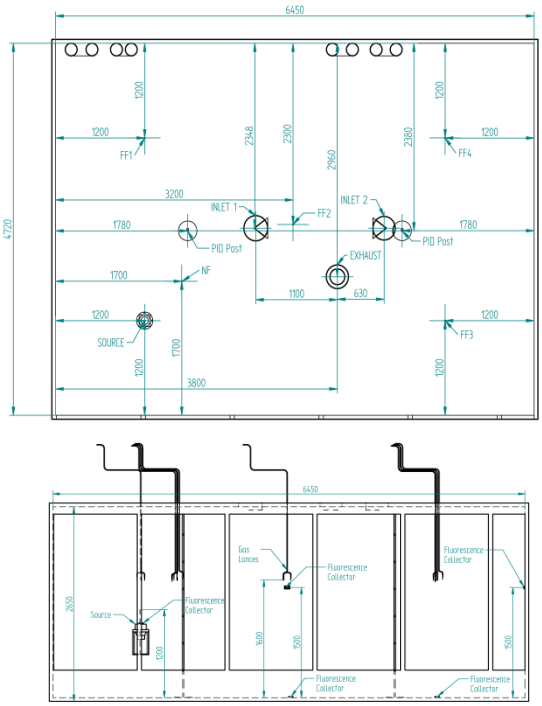

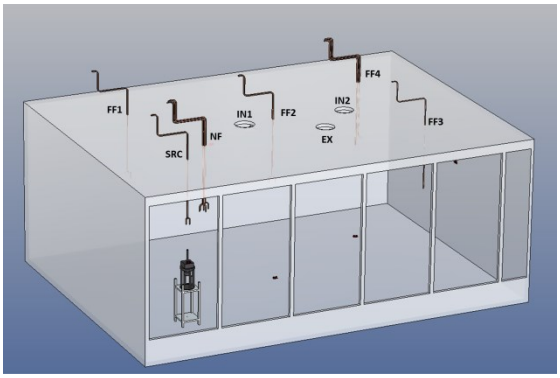

Figure 12: Top row and left: Technical drawings of the location of the source, in- and outlets, aerosol sampling lances and particle collectors. Right: Photograph of the source (front), copper sampling lances and a balometer (red) measuring the outlet airflow.

Table 4: Instruments used with location, type, serial number, owner, gas flow and residence time in a 2.60 m long gas lance of the specified tube inner diameter. CPC1 moved to a new location at the specified time. The OPC was only operated from Thursday on for oil mist experiments.

Location	ID	Type	Serial Number	Institute	Flow in slm		Tube i.d. mm	Res. Time s	Begin
					nomi-nal	on Sat 19:00			
Inlet 1	CPC1	TSI 3007	3007-06140003 3.1	ITENE	0.7	0.93	4	2.8	
Source 1	CPC2	TSI 3007	3007-01090003 3.1	BAuA	0.7	0.68	4	2.8	
Source 1 & 2	SMPS1 w/dilution	TSI 3081 TSI 3082 TSI 3088	DMA 3081A1403008 Class 3082001414001 Neutr 3088011414002	NRCWE	0.7	1.06	4	2.8	
Nearfield	CPC3	TSI 3007	3007-07110004 1.0	ITENE	0.7	0.78	4	2.8	
Nearfield	FMPS1	TSI 3091	70550213	NRCWE	10	10	8	0.8	
Nearfield	ELPi+1	Dekati ELPi+		NRCWE	10	8.4	8	0.8	
Nearfield	NSAM	TSI 3550	70552201	BAuA	2.5	2.6	4	0.8	
Nearfield	DiscMini1	MatterAerosol	101596	IOM	1.0	1.0	4	2.0	
Nearfield	OPS	TSI 3330	3330114002	ITENE	1.0	-	4	2.0	Thu 10:00
Farfield 1	SMPS2 w/source	Grimm	54301301, DMA 5LP71301	BAuA	0.3	0.32	4	6.5	
Farfield 1	CPC1	TSI 3007	3007-06140003 3.1	ITENE	0.7	0.93	4	2.8	Mon 14:07
Farfield 2	CPC4	TSI 3007	3007-02120013 3.1	NRCWE	0.7	0.7	4	2.8	
Farfield 2	FMPS2	TSI 3091	70534084	NRCWE	10	9.5	8	0.8	
Source 2	CPC8	Grimm 5.403	54300901	NRCWE	0.3	-	4	2.8	
Exhaust	CPC7	TSI 3007	3007-11140003 3.1	TNO	0.7	0.75	4	2.8	
Exhaust	FMPS4	TSI	70933232	IOM	10	9.5	8	0.8	
Farfield 3	CPC5	TSI 3007	3007-03011006 1.0	TNO	0.7	0.78	4	2.8	
Farfield 4	CPC6	TSI 3007	3007-03041000 2.0	BAuA	0.7	0.6	4	2.8	
Farfield 4	FMPS3	TSI 3091	71244057	IOM	10	9.5	8	0.8	
Farfield 4	ELPi+2	Dekati ELPi+		TNO	10	10	8	0.8	
Farfield 4	DiscMini2	MatterAerosol	101465	BAuA	1.0	1.0	4	2.0	

Table 5: Estimated particles losses in sampling pipes through deposition.

Location	ID	Flow in slm on Sat 19:00	Tube i.d. mm	Tube Reynolds number	Friction velocity (m s^{-1})	Lost fraction 10nm particles	Lost fraction 40nm particles	Lost fraction 200nm particles	Total lost fraction for typical NaCl PSD
Inlet 1	CPC1	0.93	4	360	0.20	13.0%	2.3%	0.4%	2.4%
Source 1	CPC2	0.68	4	264	0.17	15.0%	2.7%	0.4%	2.9%
Source 1	SMPS1 w/dilution	1.06	4	411	0.21	12.2%	2.1%	0.3%	2.3%
Nearfield	CPC3	0.78	4	302	0.18	14.1%	2.5%	0.4%	2.7%
Nearfield	FMPS1	10	8	1938	0.23	3.0%	0.5%	0.1%	0.5%
Nearfield	ELPi+1	8.4	8	1628	0.21	3.2%	0.5%	0.1%	0.6%
Nearfield	NSAM	2.6	4	1008	0.33	8.0%	1.4%	0.2%	1.5%
Nearfield	DiscMini1	1.0	4	388	0.20	12.5%	2.2%	0.3%	2.4%
Nearfield	OPS	-	4	-	-	-	-	-	-
Farfield 1	SMPS2 w/source	0.32	4	124	0.12	21.1%	3.8%	0.6%	4.1%
Farfield 1	CPC1	0.93	4	360	0.20	13.0%	2.3%	0.4%	2.4%
Farfield 2	CPC4	0.7	4	271	0.17	14.8%	2.6%	0.4%	2.8%
Source 2	CPC8	-	4	-	-	-	-	-	-
Exhaust	CPC7	0.75	4	291	0.18	14.3%	2.5%	0.4%	2.7%
Exhaust	FMPS4	9.5	8	1841	0.22	3.0%	0.5%	0.1%	0.5%
Farfield 2	FMPS2	9.5	8	1841	0.22	3.0%	0.5%	0.1%	0.5%
Farfield 3	CPC5	0.78	4	302	0.18	14.1%	2.5%	0.4%	2.7%
Farfield 4	CPC6	0.6	4	233	0.16	15.9%	2.8%	0.4%	3.0%
Farfield 4	FMPS3	9.5	8	1841	0.22	3.0%	0.5%	0.1%	0.5%
Farfield 4	ELPi+2	10	8	1938	0.23	3.0%	0.5%	0.1%	0.5%
Farfield 4	DiscMini2	1.0	4	388	0.20	12.5%	2.2%	0.3%	2.4%

2.5.7 *Data collection and documentation*

Data collection was started after having synchronized the instrument computer's clocks. The data were collected at regular intervals and stored into individual instrument folders. After completion of the experiments, the data were collated into one data set and chunked into separate streams according to the start and end times of the experiments. All experimental parameters and (unforeseen) occurrences were documented on paper as well as into a computer file. The instruments documented their operation parameters directly into the data files. A table of the experimental schedule with details is given in Table 6.

Instruments were checked regularly. CPCs required regular refilling of their alcohol reservoir, which, since it causes data errors, was performed during the experimental runs. Also dedicated experiments were run for comparing the monitoring instruments, see Section 2.6.1.2. However, data consistency checks were possible only sporadically due to the huge amount of incoming data. Therefore, some malfunctioning and resulting data inconsistencies were not discovered during the experiments.

2.5.7.1 *Data formatting and chunking*

The recorded data were downloaded from the computers in text format and converted to matrices using Matlab scripts. For each instrument, a separate CSV file was generated which consists of data from the whole measuring week. Both Matlab and CSV files were formatted in the same way. For the CPC, the first column contains the time vector, the second the measured concentration. For the SMPS, FMPS, ELPI, OPS and NSAM, the first row consists of two positions of NaN followed by the logarithmic bin centre in nanometres. The first column contains again the time vector, the second column the total number concentration. The rest of the columns contain the particle number concentrations normalised to the logarithmic bin size (dN/dlogDp) of the respective bins.

2.5.8 *Type of experiments performed*

A series of experiments was designed and performed focusing on the chamber airflow characteristics, the distribution dynamics of locally generated aerosols with respect to their concentration and particle size, as well as wall deposition probabilities and the coagulation propensity of aerosols with a particle background.

2.5.8.1 *Age of air*

The air change effectiveness can be characterized by the concept of local age of air, and thus be compared to CFD predictions. The mean age of air at point p correspond to the average time needed by air molecules to reach the point p, starting from the air inlets.

For the present joint experiment, the step-down method was used. It consisted in marking the supplied air with a tracer (ethanol vapours) until a steady-state concentration C(p,0) was reached at each point p in the room. Then at time t=0, the tracer injection was stopped and the time dependent decay of tracer concentrations C(p,t) was recorded at the chosen measurement points, until the background level of tracer C(p,∞) was reached.

The mean age of air $\tau(p)$ at point p is then given by computing the integral:

$$\tau(p) = \int_0^\infty \frac{C(p,t) - C(p,\infty)}{C(p,0) - C(p,\infty)} dt$$

The mean age of air at several points in the room was thus measured for the air exchange rates of 3.5 and 10 vol./h.

Twelve measurements points, numbered from 1 to 12, were placed as shown on Figure 13.

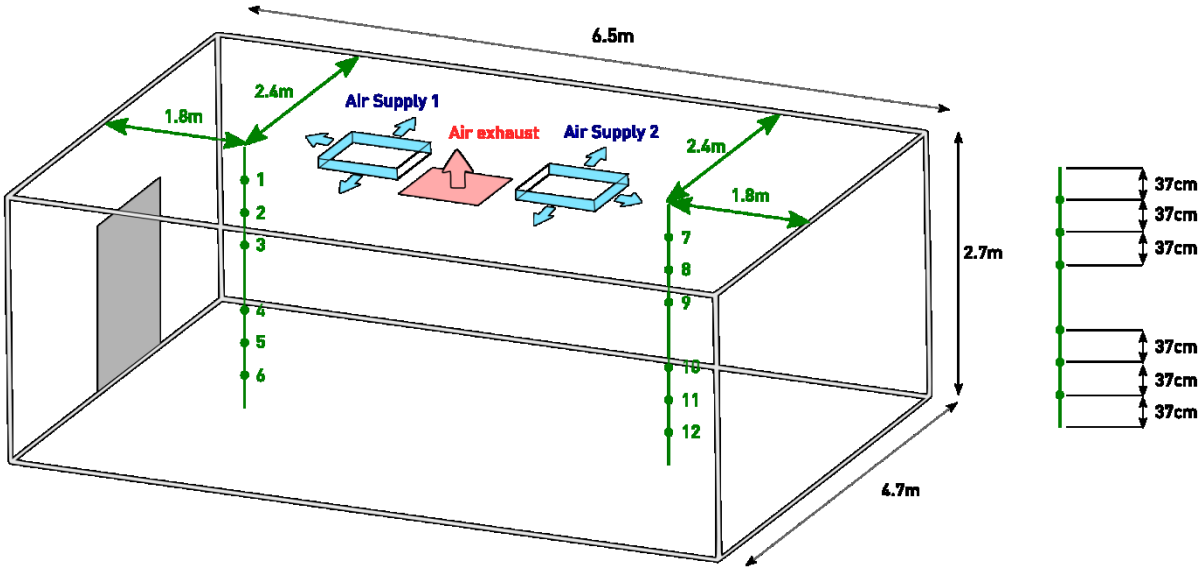

Figure 13: Age of air / PID measurement points location.

2.5.8.2 *Tracer gas distribution*

In addition to age of air measurements, tracer gas was also used to compare the efficiency of ventilation in removing a gas and an aerosol of nanoparticles, in order to highlight a possible specific behaviour of airborne nanoparticles. For this experiment, tracing gas (N_2O) was injected directly with the nanoparticle sources, in the ejector of the PALAS AGK 2000 nebulizer.

N_2O sampling probes were placed at the different NF and FF measurement points chosen for the experiment, and tracing gas concentrations were monitored simultaneously with nanoparticles data, using the photoacoustic detector evoked before.

2.5.8.3 *Aerosol sampling*

Aerosol sampling was performed through gas lances made from flexible copper tubes, as described in section 2.5.6 in “human nose height”. The tube diameter was chosen according to the gas sampling flow of the instruments.

2.5.8.4 *Surface sampling*

Deposition samples were collected during three tests: The test with SiO_2, and two with sodium fluorescein. For the test with SiO_2, only the carbon samplers were used. For the test with Na fluorescein at ventilation rate 10 only polycarbonate samplers were used for analysis with fluorescence spectroscopy. For the test with Na fluorescein at ventilation rate 3.5 both carbon and polycarbonate samplers were used. Only this last test provided usable results.

For comparison with deposition samples, aerosol samples for TEM analysis on copper lined holey TEM grids were taken from the air near the source with an Ecomésur mini particle sampler (see Figure 9). The samplers were distributed as shown in Figure 14.

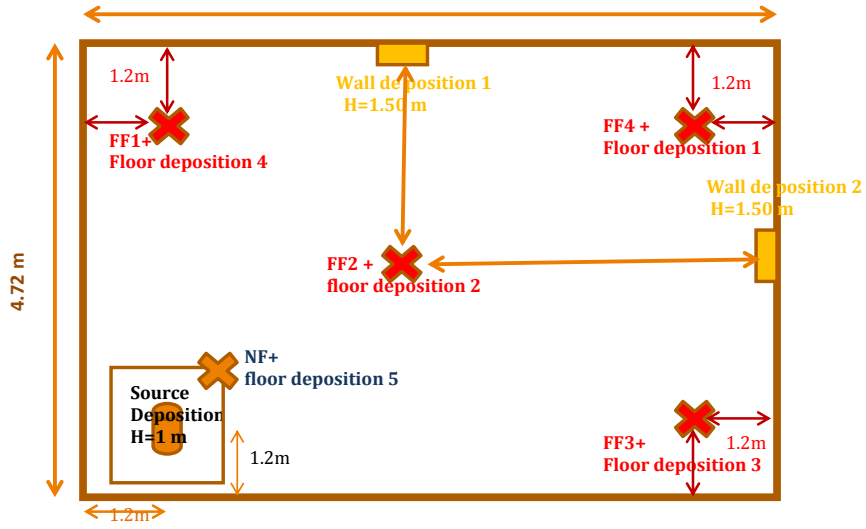

Figure 14: Locations of surface sampling.

2.5.9 *Experimental schedule*

The experimental schedule and the most important details are given in Table 6. It allows to chunk the data stream into individual experiments by specifying official start and end times and to interpret special events in the data, like spikes of the experiments.

Table 6: Experimental schedule of March 2015.

Day		Task	ID	Experiment		Material	Source				Ventilation		
				Start	End		Type	Pattern	Start	Stop	Rate	Start	Stop
20	**Friday**	Unpacking & Installation	**-**	Fri 10:00	Sat 20:00	-	-	-	-	-	-	-	-
21	**Saturday**	Air flow calibration	**-**	Sat 10:00	Sat 14:50	-	-	-	-	-	-	-	-
		Inter-comparison	**DTU01**	Sat 19:50	Sat 20:15	NaCl 0.1 wt.%	10 slm Palas AGK	Constant	19:55	20:14	0		Sat 19:50
22	**Sunday**	Inter-comparison	**DTU02**	Sun 19:54	Sun 23:59	NaCl 0.1 wt.%	10 slm Palas AGK	Constant	17:06	19:58	0		Sun 19:54
23	**Monday**	Stationary at high exchange rate	**DTU03**	Mon 13:35	Mon 14:53	NaCl 0.1 wt.%	10 slm Palas AGK	Constant	13:35	14:23	10	Mon 09:23 Rate 10	
		Stationary at high exchange rate	**DTU04**	Mon 15:10	Mon 16:40	NaCl 0.1 wt.%	10 slm Palas AGK	Constant	15:10	15:50	10		
		Inter-comparison	**DTU05**	Mon 16:48	Tue 04:00	NaCl 0.1 wt.%	10 slm Palas AGK	Constant	16:56	17:45	0		Mon 16:48
24	**Tuesday**	Stationary at low exchange rate	**DTU06**	Tue 09:32	Tue 13:35	NaCl 0.1 wt.%	10 slm Palas AGK	Constant	09:32	12:11	3.5	Tue 08:10 Rate 3.5	
		Stationary at low exchange rate	**DTU07**	Tue 13:36	Tue 16:30	NaCl 0.1 wt.%	10 slm Palas AGK	Constant	13:36	15:06	3.5		
		Stationary at low exchange rate with addition of tracer gas	**DTU08**	Tue 18:30	Tue 19:30	0.1 wt.% Na-fluorescein	10 slm Palas AGK	Constant	18:30	19:00	3.5		
25	**Wednesday**	Spiking	**DTU09**	Wed 09:45	Wed 13:07	NaCl 0.1 wt.%	10 slm Palas AGK	Spiking	09:45, 10:01, 10:17, 10:33, 10:49, 11:05, 11:21		3.5	Wed 08:00 Rate 3.5	
		Spiking	**DTU10**	Wed 13:34	Wed 14:50	NaCl 0.1 wt.%	10 slm Palas AGK	Spiking	13:37, 13:40, 13:43, 13:46, 13:49, 13:52, 13:55, 13:58, 14:01, 14:04		10	Wed 13:07 Rate 10	
		New source position and tracer gases Age of Air	**DTU11 AoA04**	Wed 15:34	Wed 17:10	NaCl 0.1 wt.% EtOH, N_2O	10 slm Palas AGK EtOH: 4 bar N_2O: Gas bottle	Constant Age of air : step down	15:31 EtOH 15:31 N_2O	16:20 EtOH 16:38 N_2O	10		
		Age of Air	**AoA05**	Wed 17:37	Wed 20:21	NaCl 0.1 wt.% EtOH, N_2O	EtOH: 4 bar	Step up and down	17:37 EtOH	18:51 EtOH	3.5		
		Fluorescence	**DTU12**	Wed 18:52	night	0.1 wt.% Na-fluorescein	10 slm Palas AGK	Constant	18:57	08:00 +1d	3.5		
26	**Thursday**	Coagulation	**DTU13**	Thu 10:00	Thu 13:00	NaCl 0.1 wt.% + Oil mist	NaCl: 10 slm Palas AGK Oil: 10 slm Palas AGF	Constant	10:26 Oil 11:04 NaCl	12:40 NaCl 13:00 Oil	3.5		
		Silica	**DTU14**	Thu 13:23	Thu 17:26	Silica	FhG Generator	Constant	14:56	16:24	3.5		
		Oil mist characterization	**DTU15**	Thu 13:52	Thu 14:45	Oil mist	Oil: 10 slm Palas AGF	Constant			3.5		
27	**Friday**	Deinstallation & Packing	-	-	-	-	-	-	-	-	-	-	-

This project has received funding from the European Union Seventh Framework Programme (FP7/2007-2013) under grant agreement no 310584

2.6 Results

The main results of the joint experiment are described in the following.

2.6.1 *Performed preparatory experiments*

The airflow dynamics of the chamber was studied by a series of age-of-air experiments using tracer gases. Also the instrument inter-comparability was evaluated.

2.6.1.1 *Age of air experiments*

The measured normalized decay functions $C^*(p,t)$ of Ethanol concentration for the 12 points are shown on Figure 15 and Figure 16, for the air exchange rates of 3.5 and 10 vol./h, where $C^*(p,t)$ is given by :

$$C^*(p,t) = \frac{C(p,t) - C(p,\infty)}{C(p,0) - C(p,\infty)}$$

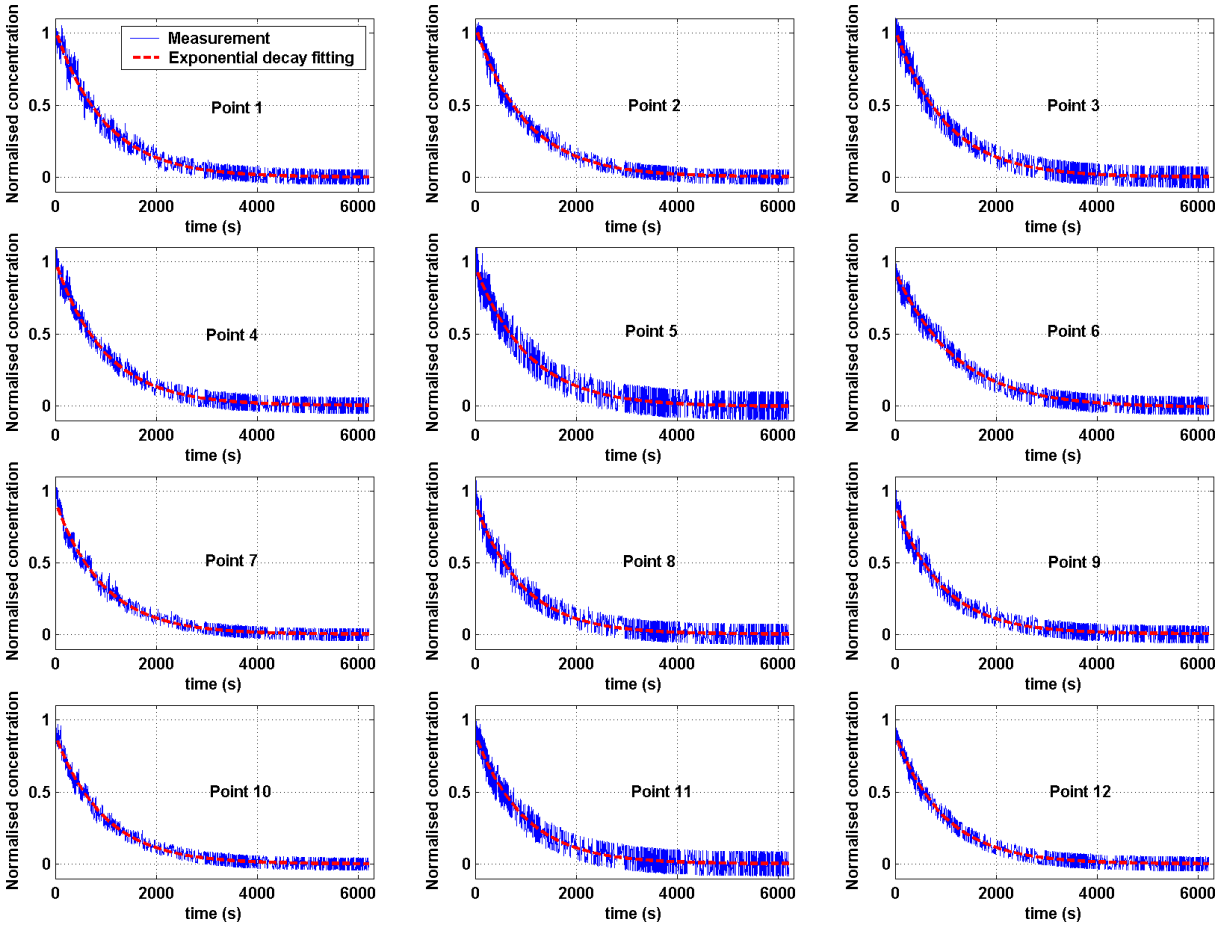

Figure 15: Normalized concentration decay functions at the 12 Age of Air measurement points for a 3.5 vol./h air exchange rate in the room.

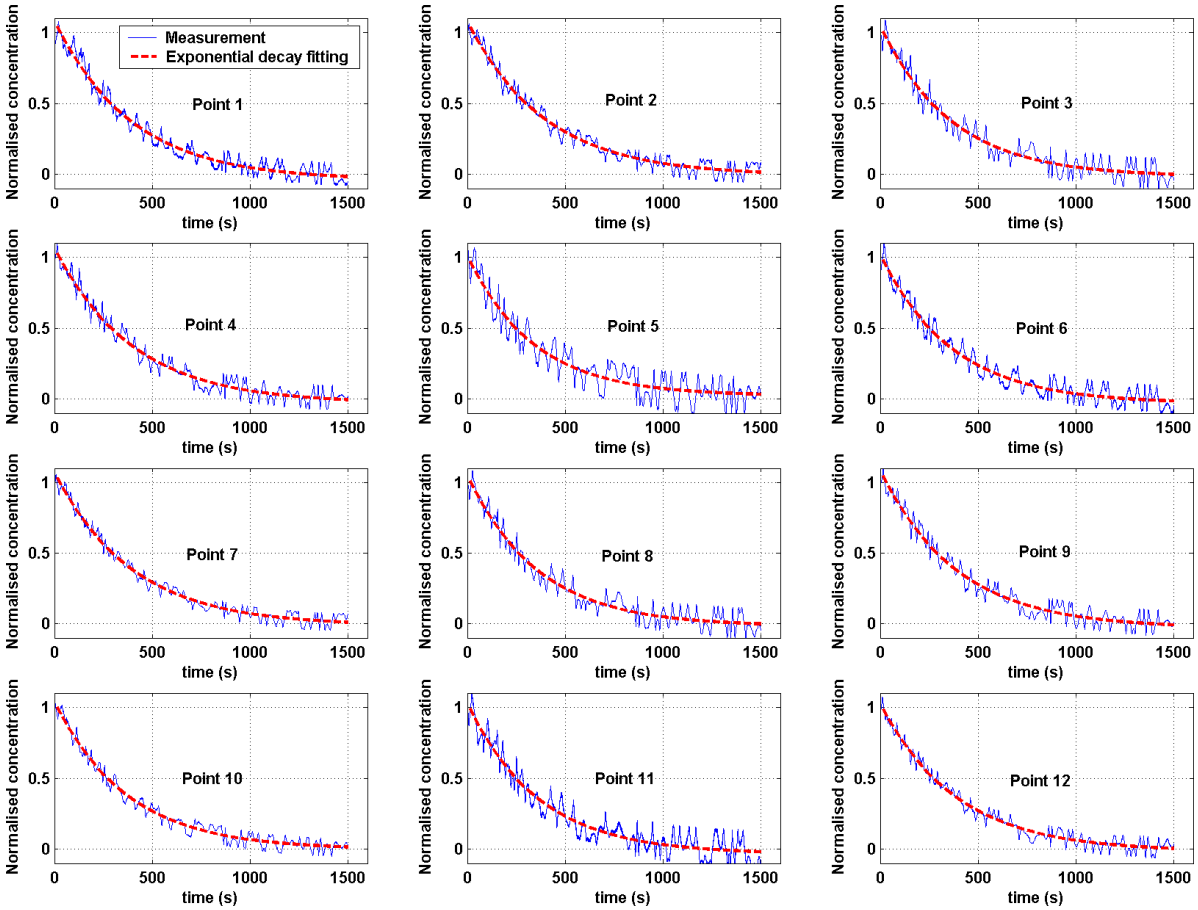

Figure 16: Normalized concentration decay functions at the 12 Age of Air measurement points for a 10 vol./h air exchange rate in the room.

These decay functions allow computing the mean age of air at the 12 measurement points, either by computing their integral or by fitting an exponential decay function such as shown on the figures.

The corresponding mean age of air are thus reported in Table 7, the perfect mixing time constant in the room being also reported for comparison.

For these measurements, it is believed that fitting an exponential decay function to compute the mean age of air is more robust since it is less sensitive to estimates of $C(p,0)$ and $C(p,\infty)$.

Table 7: Mean age of air measured at each point in seconds.

Air Ex. rate		Sensor #												Perfect mixing time constant (s) V/Q
	Method	1	2	3	4	5	6	7	8	9	10	11	12	
3.5	Integral (s)	1013	1058	1030	999	985	1054	897	876	876	866	867	875	1029
	Exp.Decay (s)	990	1003	999	981	1039	1189	945	933	923	960	953	967	
10	Integral (s)	370	406	355	381	365	332	399	354	379	375	326	370	360
	Exp.Decay (s)	392	396	363	398	339	367	394	359	388	369	361	388	

These measurements show that a good mixing of air occurs in the room, at least at the chosen points: the mean age of air does not vary much from its mean (20% of maximum deviation at 3.5 vol./h and 10% at 10 vol./h), and the age of air is always very close to what it should be if the room were perfectly mixed (within 15% at 3.5 vol./h and within 11% at 10 vol./h). These results then appear very consistent with the ventilation setup.

2.6.1.2 *Instrument inter-comparison experiments*

The general agreement of the concentration measurements of the various devices positioned at the different locations was tested by long-term experiments in a closed chamber without ventilation or source operation. After a residence time of about an hour, it was assumed that the aerosol distribution inside of the chamber had approached equilibrium sufficiently well.

Figure 17 show the high degree of pair-wise linear correlation with offset of the instrument number concentration readings during its decrease after closing of the chamber door with sources and ventilation switched off. The degree of linear correlation exceeded in all cases $R = 0.98$. The absolute concentrations, however, i.e. the slopes of a linear regression without offset of the instrument readings to a reference instrument, vary significantly as Figure 18 shows, and reveals the ELPI+ placed in the far field 4 (FF4) to be beyond an acceptable deviation.

The FMPS at the exhaust was obviously affected by a local intake of outside air during experiment E02 since it concentration measurement did not fall below 1800 cm^{-3}, whereas the other devices recorded minimum concentrations well below 500 cm^{-3}.

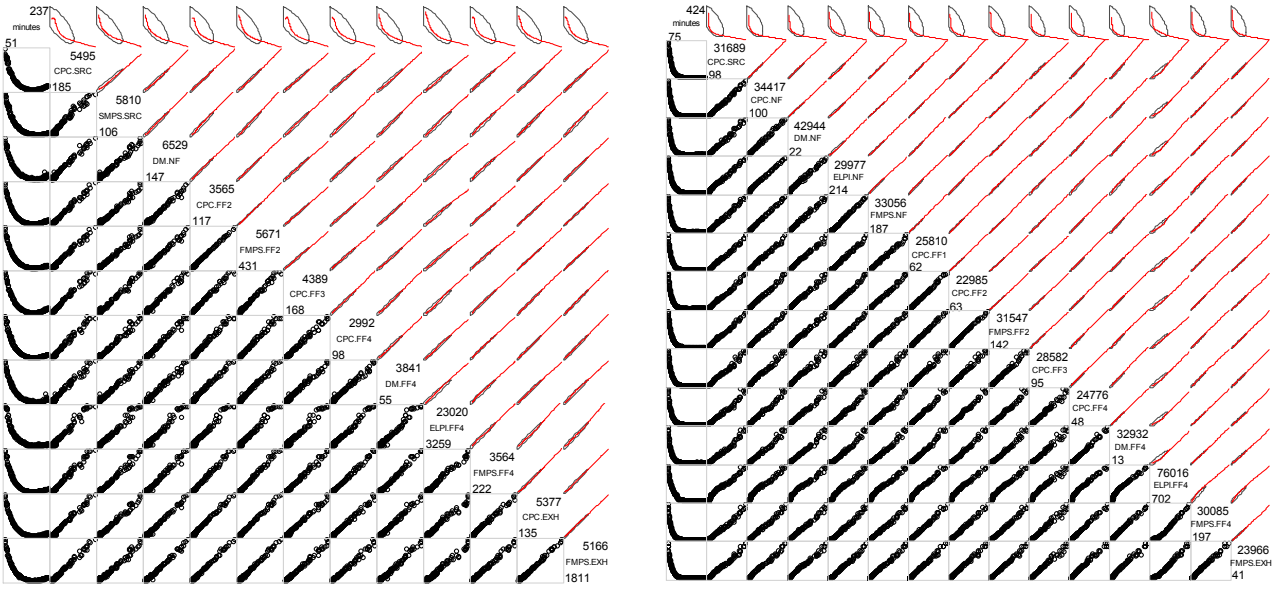

Figure 17: Correlation diagrams for the time series of experiment E02 (left) and E05 (right) starting 50 (E02) and 75 minutes (E05) after closing of the chamber door. The decrease of particle number concentration was measured inside of the closed chamber without ventilation. The centre diagonal gives the name of the instrument and its location together with the maximum and minimum value. The lower triangle of the matrix show pair-wise correlation plots. The upper triangle shows LOESS-smoothed pair-wise data interpolations and overlaid 1-sigma ellipses.

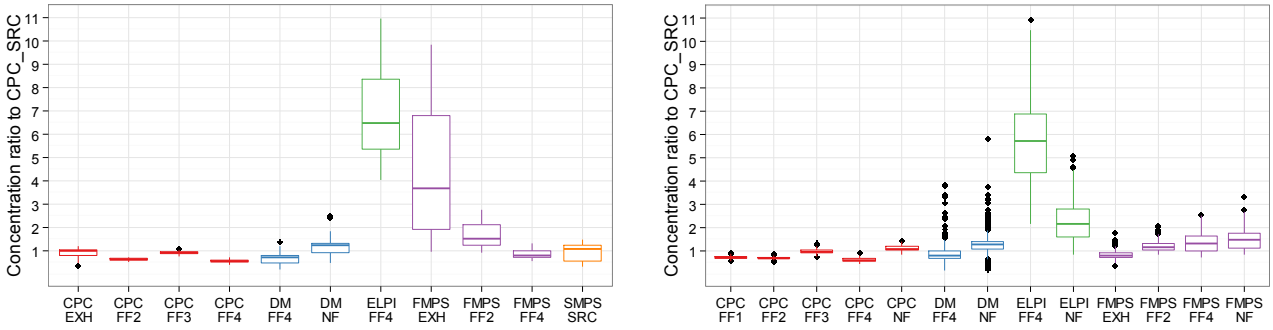

Figure 18: Box plots of the instrument readings vs. the CPC_SRC readings for experiment E02 (left) and E05 (right).

2.6.2 *Performed exposure experiments*

A series of experiments was conducted using source strength-calibrated nanoparticle emitters. By a detailed mapping of the aerosol concentration at the different sampling locations, the chamber aerosol dynamics was studied. The experiments also simulated different exposure scenarios that were considered typical for workplaces handling MNMs. Part of the data was also usable for inter-comparison experiments of the monitoring instruments. The studied exposure scenarios included stationary emission, transient spiking and bimodal coagulation conditions at no, intermediate and high air exchange.

2.6.2.1 *Source position variation experiments*

The influence of source position on particle concentrations throughout the room was studied experimentally for an air exchange rate of 10 Vol.h^{-1}, for a steady emission rate of NaCl nanoparticles. In experiment E3 and E4 (repetition of the same experiment), the source was placed at its reference position, while in experiment E11 it was moved directly below the exhaust position.

Figure 19 shows a comparison of particles total number concentrations between the 3 experiments, at various locations in the room (FF1, FF2, FF3 and FF4). The same emission scenario was considered in these 3 experiments: the source is first started in continuous regime (step-up signal), then a steady-state concentration plateau is reached everywhere in the room, and the source is stopped (step-down) which lead to a decay of concentration.

Comparisons of measurements between the different experiments indicate a good repeatability between E3 and E4, meaning that the experimental set-up was well mastered. In steady state regime, concentrations fluctuate significantly with time, which shows the influence of turbulence of airflows on pollutant transport. Note that between experiment E3 and E4, the sources were not switched off after the same duration, which lead to the de-synchronised concentration decay in Figure 19.

In experiment E11, the concentrations in the room were significantly lower. This can easily be explained by the placement of the source below the exhaust: An important part of the emitted particle is directly evacuated by the exhaust before being mixed in the room atmosphere and reaching the various particle counters.

When comparing the time series of detectors with different distance to the source, a broadening of the aerosol injection profile can be observed. Despite to the complexity of the aerosol dynamics, this broadening can, in a first order approximation, be reproduced by convoluting in time t the source emission profile with a solution of the three dimensional diffusion equation of the form $\frac{x}{\sqrt[3]{4\pi D\, t}}\, e^{-\frac{x^2}{4D\, t}}$ and iteratively fitting the effective distance x to maximise the correlation of the two time series, see Figure 20. This distance x should be related to the air exchange rate-affected

distance between source and detector. During the fit, also a time lag was admitted to account for long transport times to more distant detectors, but only very small time shifts, generally below ± 2 minutes, were required and could not be fitted reliably since devices were synchronisable with 1 minute accuracy only, due to the lower time resolution of the SMPS. Since the SMPS was directly connected to the source, the emitted profile was recorded without spatial diffusion effects.

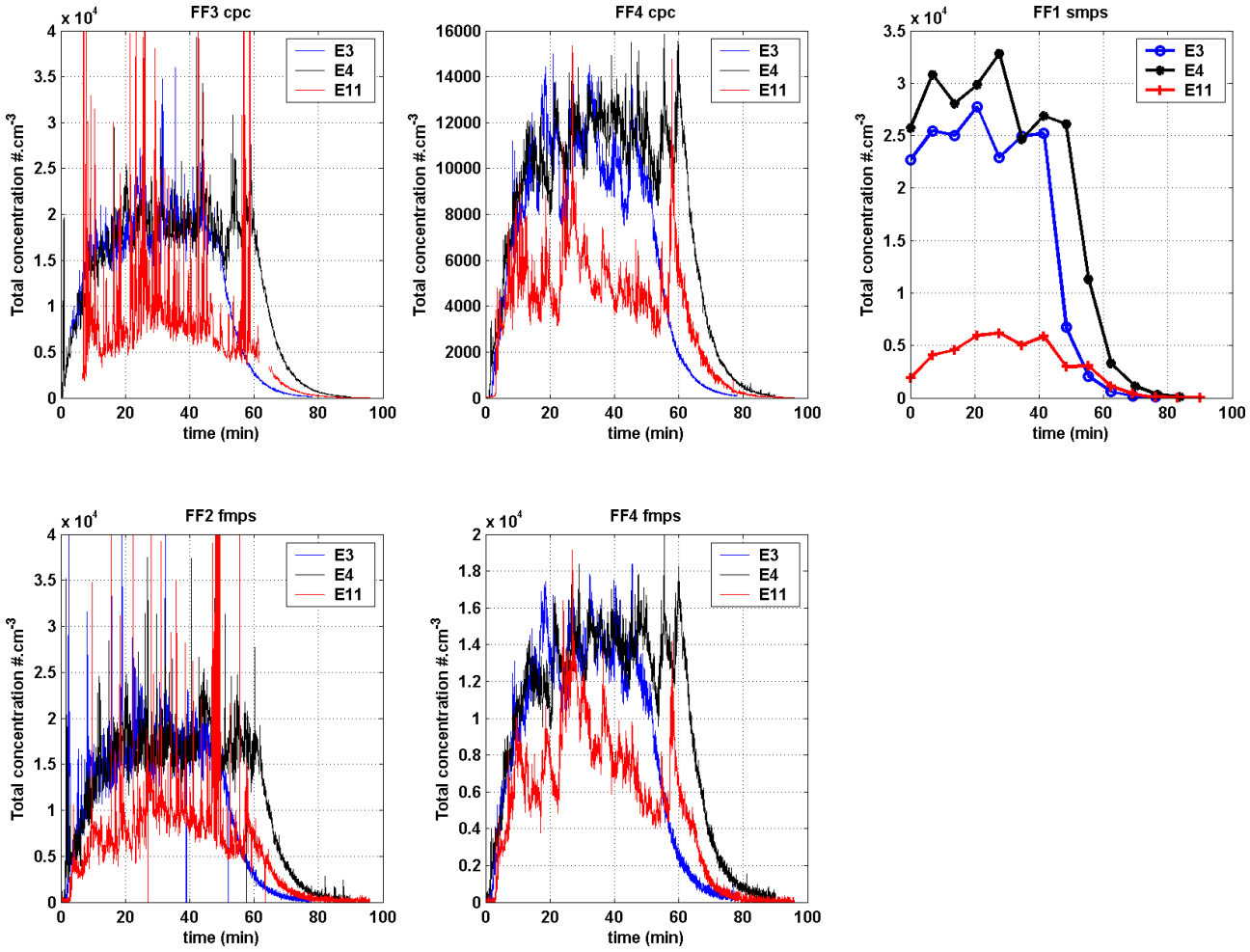

Figure 19: Time evolution of particles total number concentration at different locations in the room: influence of moving the source between experiment E3,E4 and E11.

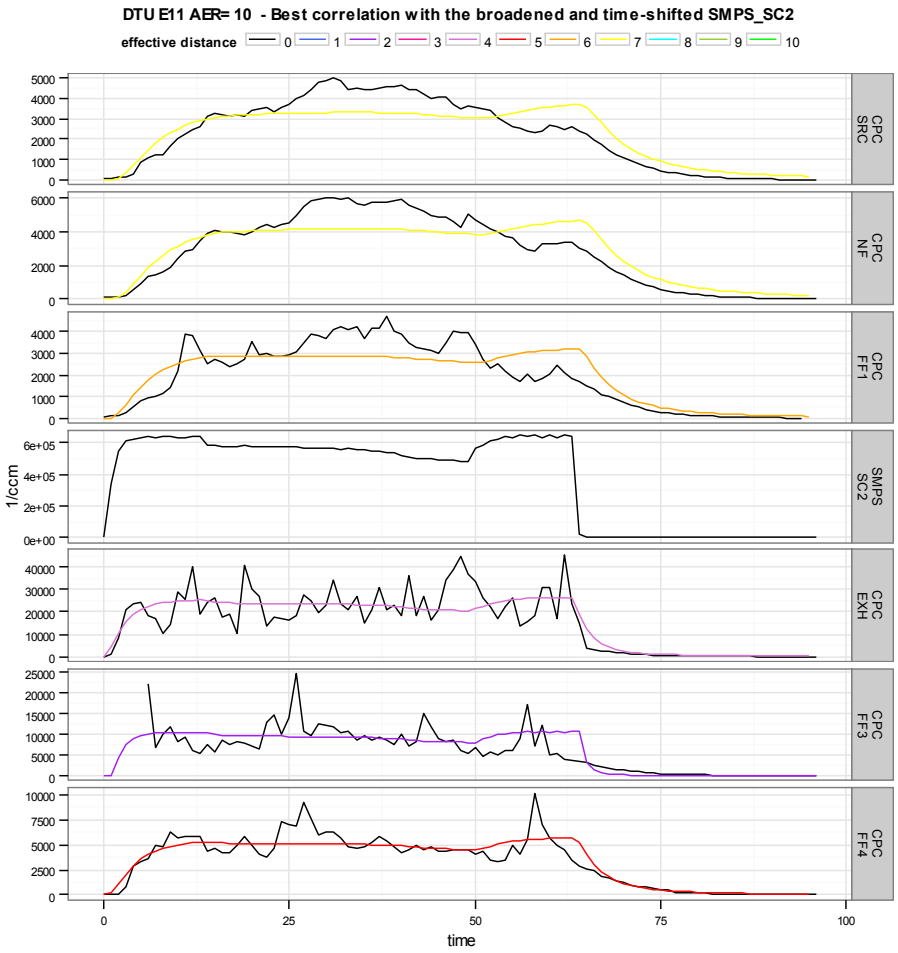

Figure 20: Experiment E11 particle number concentration data from CPCs and the SMPS directly connected to the source below the exhaust. The data was averaged by a running mean of 1 minute. The overlaid curves result from fitting the (colour coded) effective distance of a solution of the diffusion equation that was used for convoluting the SMPS_SC2 time series.

2.6.2.2 *Spiking experiments*

Experiment 9 and 10 (E9 and E10) were dedicated to emission scenarios where the nanoparticles are released as spikes. In E9, seven emission spikes of 60 seconds and separated by 900s were released in the room (air exchange rate of 3.5 Vol.h^{-1}), from the nebulizer fed with a 0.1% NaCl solution with a carrier airflow at 10 slm. In E10, the air exchange rate was 10 Vol.h^{-1} and ten 60s spikes separated by 120s were released.

Figure 21 illustrates the time evolution of particles total number concentration (and PSD for FMPS) at different locations in the room for experiment E9. The effect of emission spikes on the aerosol concentration is clearly visible, as concentration peaks appear regularly consecutively to emission spikes. Compared to spikes, the concentration peaks appear broadened through (turbulent) diffusion.

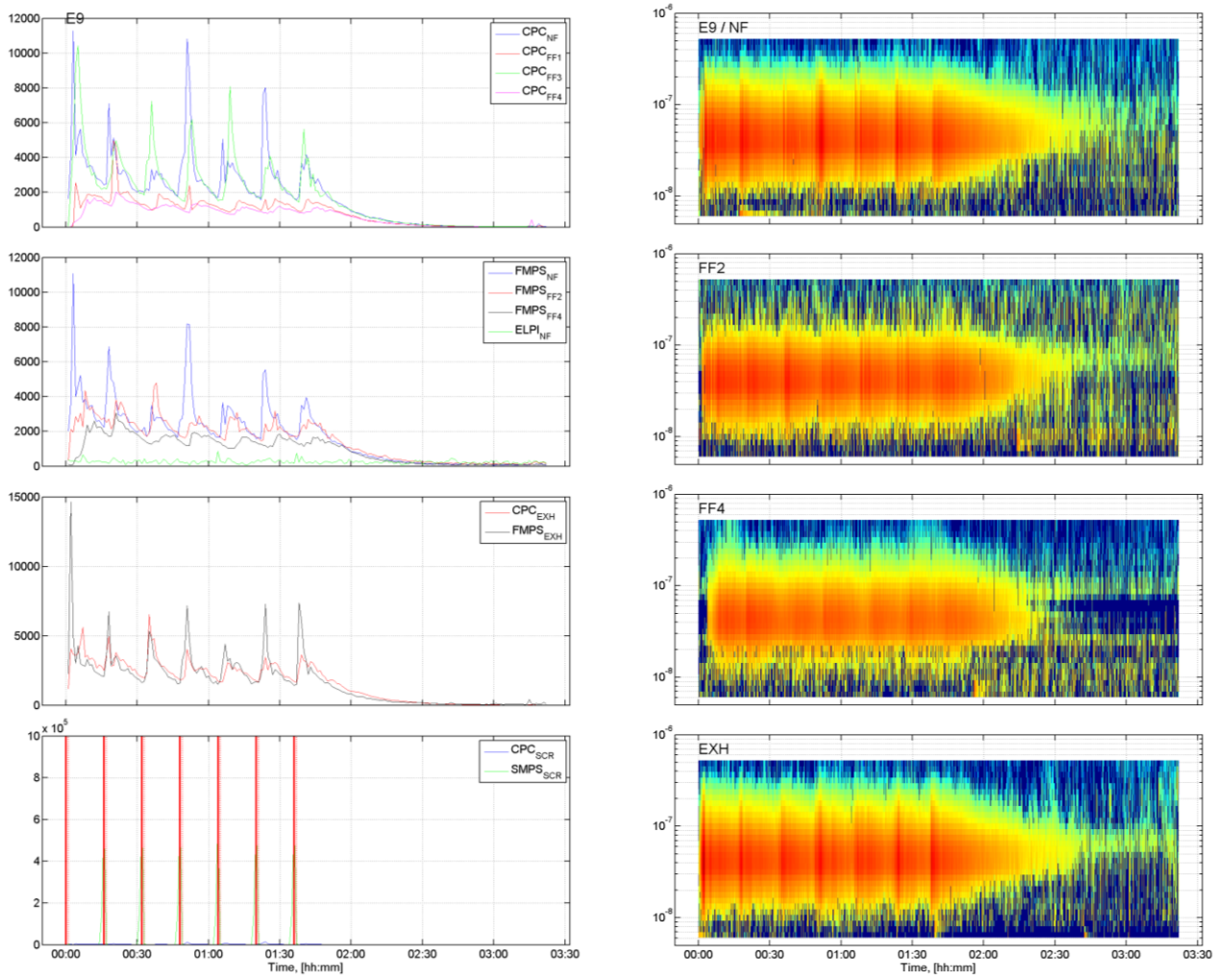

Figure 21: Data of the spiking experiment DTU09 with NaCl at different locations inside of the chamber.

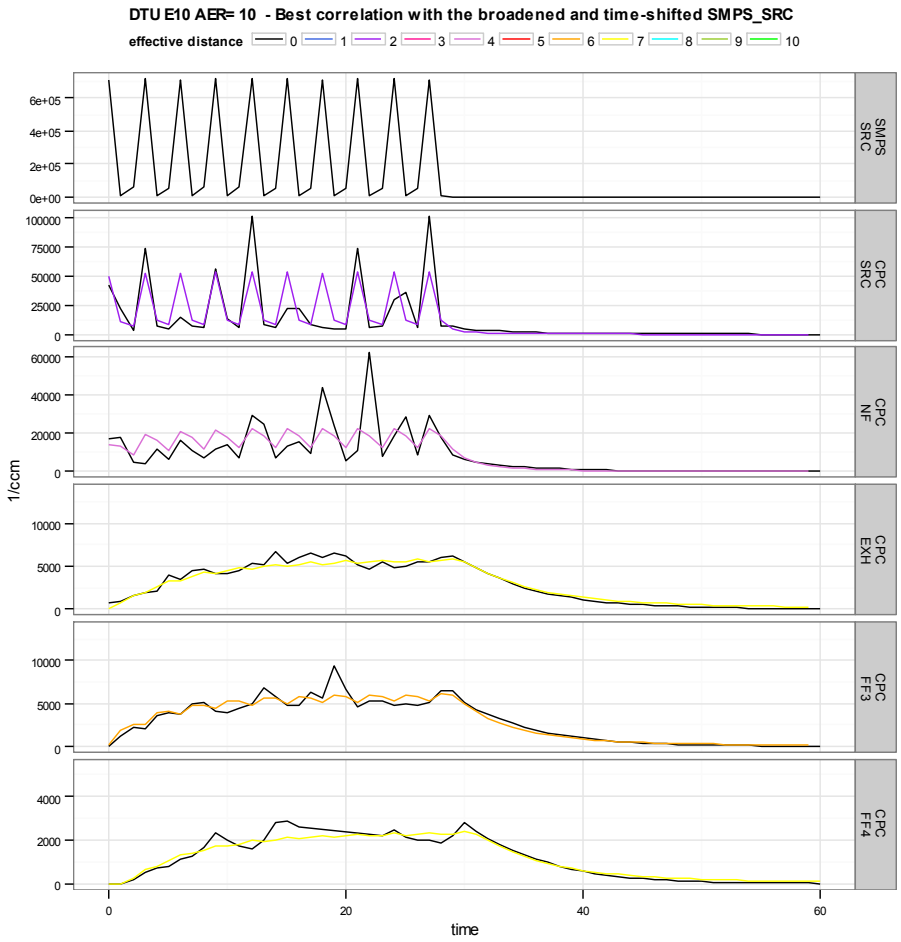

Figure 22: Spiking experiment E10 particle number concentration data from CPCs and the SMPS directly connected to the source. The data was averaged by a running mean of 1 minute. The overlaid curves result from fitting the (colour coded) effective distance of a solution of the diffusion equation that was used for convoluting the SMPS_SRC time series.

As was described in Section 2.6.2.1, the broadening of the initial spike pattern can, in a first order approximation, be reproduced by convoluting in time the spike with a solution of the three dimensional diffusion equation and iteratively fitting the effective distance x, see Figure 22. This distance x should be related to the air exchange rate-affected distance between source and detector. Since the SMPS was directly connected to the source, the emitted spikes were recorded without spatial diffusion effects.

2.6.2.3 *Coagulation experiment*

Coagulation experiments were done to see the effect of injecting SIO_2 nanoparticles when an existing background aerosol is already present. In this case we used atomized olive oil as background aerosol (see **Error! Reference source not found.**). After the background aerosol was table and the aerosol in the chamber was well mixed, SiO_2 particles were dispersed in the chamber. Figure 23 shows the distributions measured at different times during the experiment. Figure 24 shows the evolution of the size distributions as measured by ELPI and FMPS in the near and far field. Both figures suggest that the background aerosol concentration was not high enough to significantly affect the aerosol size distribution during the experiments. However, more detailed statistical analysis may reveal changes on small scale.

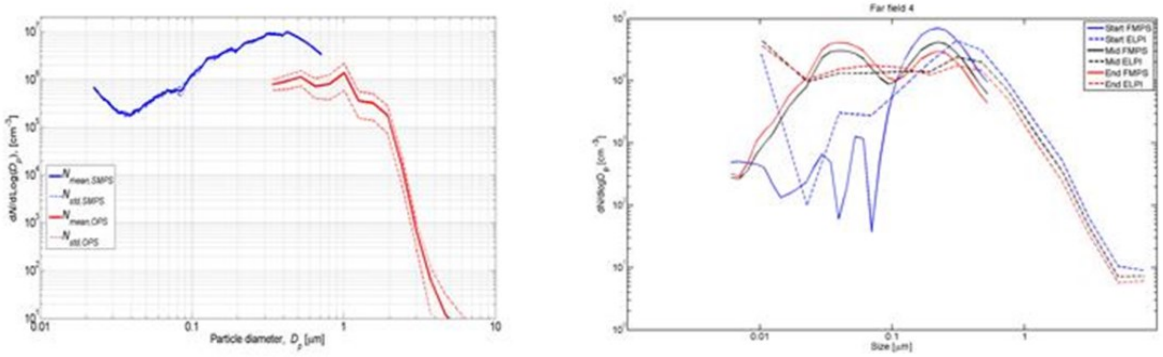

Figure 23: The left plot shows oil droplets number size distribution spectrum measured with SMPS and OPS. The right plot presents the number size distribution development during the combined oil and silica experiment.

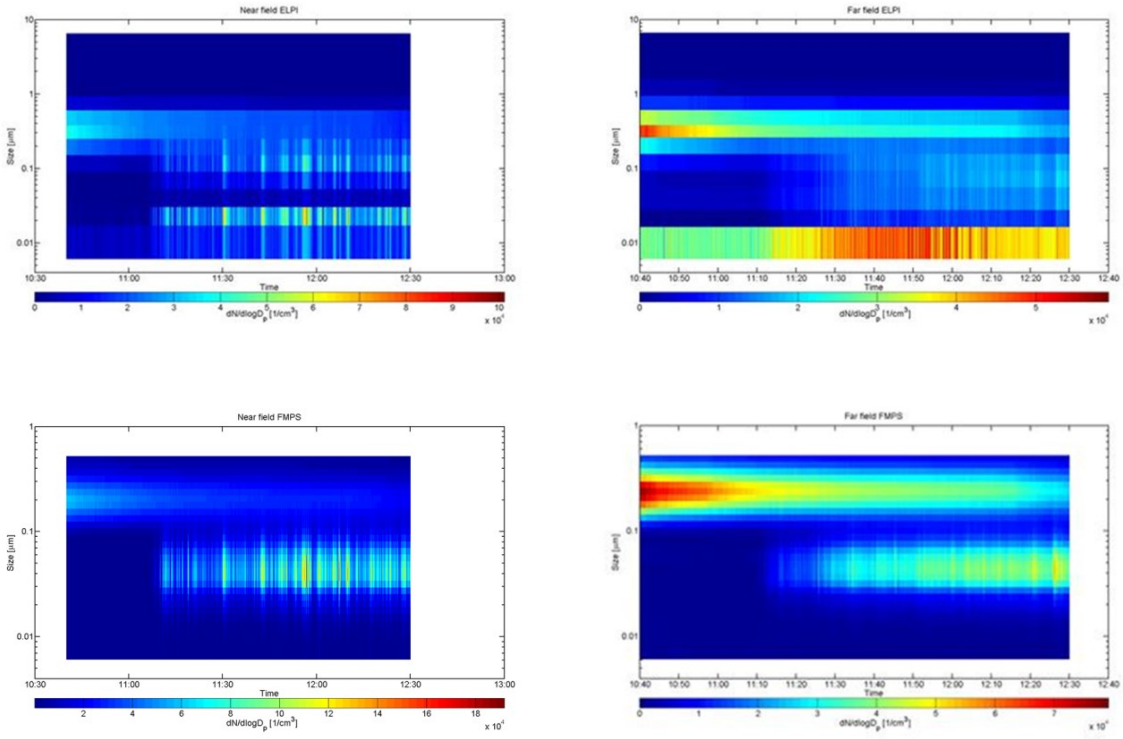

Figure 24: The plots in the upper row show the number size distribution from near field (left) and far field (right) positions as measured by ELPI. The plots in the lower row show the corresponding results as measured by FMPS.

2.6.2.4 *Deposition Results*

Deposition of SiO_2 was evaluated on sticky carbon tabs. These samples showed no particles even in the samples taken near the source, despite the fact that aerosol samples taken near the source with the MPS (and SMPS and ELPI+) showed fairly high particle concentrations.

The same observation was made for the deposition of fluorescein particles on carbon tabs. However, on the white plastic holder for the source samples and on the polycarbonate membrane source sample some orange deposition could be seen after the experiment at ventilation rate 3.5. Hence the polycarbonate samples were analysed first with SEM before they were extracted in 2 ml of demineralized water and analysed with fluorescence spectrometry (480 nm in, 530 nm reflected). The results are summarized in Table 8. Spectroscopic analysis of the samples taken at a ventilation rate of 10 times per hour showed concentrations at (source) or below the detection limit (all other samples) of 3 µg/m^2. SEM analysis of these samples did not provide any additional information.

The difference between deposition on the conducting carbon and on the insulating polycarbonate surfaces indicates that electrostatic forces played an important role in the deposition.

Table 8: Quantitative results of Na-fluorescein particle deposition at ventilation rate 3.5/hr.

Sample	Particle diameter (nm)	*Area coverage (%)*	Concentration mg/m^2
source	125	10^{-8}	1.98
NF	118	$6.2x10^{-10}$	0.60
FF2	115	$2.9x10^{-10}$	0.15
FF3	118	$6.4x10^{-11}$	0.24
FF4	-	$< 10^{-12}$	0.07
Wall 1	-	$< 10^{-12}$	0.19
Wall 2	± 60	10^{-12}	0.04

2.7 Discussion

In the following, only aspects concerning data completeness and integrity are discussed. A comprehensive interpretation of the data will be published as a peer-reviewed article.

2.7.1 *Data quality*

Technical problems during the simultaneous operation of up to 18 instruments caused some data gaps and irregularities. Corrupted data were flagged and listed in a table. For assessing the comparability of the data, dedicated inter-comparison experiments were performed.

The general agreement of the concentration measurements of the various devices positioned at the different locations was tested by long-term experiments in a closed chamber without ventilation or source operation.

A high degree of pair-wise correlations always exceeding $R = 0.98$ was found. The relative instrument errors for concentration measurement were in the order of 30-50 % and better. This is in close agreement to the manufacturers' specification of 30 %. The ELPI+ instruments, however, showed larger deviations with respect to CPC particle count rates. This will need to be considered during further interpretation of the data. The deviations appear to be partially due to an overestimation of the background count rate by the ELPI+.

Age of air measurements gave results consistent with a mixing ventilation installation, such as would be expected given the design of the experiment. The concentration when flushing the room always followed an exponential decay, which is typical of perfect mixing through ventilation, and the age of air was found homogeneous and close (by less than 15%) to the perfect mixing time constant of the room for the two tested air exchange rates.

When performing continuous-source experiments, each experiment was repeated twice for each texted air exchange rate (3.5 and 10 $vol.h^{-1}$). Mean concentration levels reached at the different locations in the room were always found repeatable, thus indicating a good control of the experimental conditions.

2.7.2 *Identified data gaps*

Following is a list of missing data and times when data are missing or were corrupted due to technical or human mistakes.

Data gaps:

- The inlet air quality was only controlled with CPC1 during the initial phase of the experiment to check the HEPA filters' performance. The concentration was always below 3 particles per cm^3.
- CPC6 at far field 4 from 2015-03-21 20:10 to 2015-03-23 10:12
- CPC7 at the exhaust from 2015-03-23 10:22 to 2015-03-24 09:00

Other aspects:

- The DiSCmini at far field 4 was not synchronised correctly and needs a time shift of about 10 minutes.
- For experiments E2 to E7, the source was not monitored properly, an ad-hoc dilution system being used upstream of the SMPS1 dedicated to source monitoring: the dilution rate was not well determined and varied between experiments. This does not lead to major drawbacks however, given the stability and repeatability of the source used, and given also

that the setup still allowed detecting instabilities of the source generation rate, even if the absolute concentration emitted could not be properly measured. Starting with experiment E8, a PALAS VKL 100 diluter was used.

2.8 Evaluation and conclusions

2.8.1 *Use of data to understand determinants of exposure*

High quality nanoparticle concentrations measurements were collected within a controlled exposure chamber under different release and ventilation conditions. These data can be used to investigate the impact on particle concentrations of a number of key determinants of exposure, namely the emission pattern and the ventilation set up, as well as characterising the temporal and spatial variability of the particle concentration. These are important factors when estimating worker's exposure.

Some of the questions of interest that could be investigated include:

- How does the concentration vary within the room? (Does the concentration at source significantly differ from the concentration in the near-field and various far-field measurements?)
- Is this difference the same regardless of the exposure scenario?
- If not, do any of the factors that were varied in the experiments help to explain how the concentration differs between source, near-field and far-field?
- How does the ventilation rate affect the concentrations in the room?

Understanding better how measurements taken can relate to actual exposures experienced by workers is extremely valuable in progressing exposure assessment of nanomaterials.

However, it is clear that measurements were carried out under controlled test conditions with the aim to evaluate the performance of quantitative two-box models and although attempts were made to ensure realistic release and ventilation conditions, the measured concentration levels are not necessarily representative of exposures experienced by workers in manufacture or use of engineered nanomaterials.

2.8.2 *Use of data to test quantitative exposure models*

Data generated during these experiments will be used to evaluate the performance of quantitative exposure tools by comparing the predictions in the near and far field to those that were measured. This will give an idea of the accuracy of the the model predictions. In addition, consideration of the variation in the measured far-field concentration levels will provide some evidence on the uncertainty bounds that may need to be considered for scenarios that are similar to the experimental conditions. However, it will not be possible to extrapolate these uncertainties to the near field predictions. Additional experiments will be required to determine the spatial variation of the particle concentration in the near field, although the CFD modelling approach may provide some insight too.

The deposition samples can be used to test the corresponding factors within the models, to some extent. As the two-box model provides one estimate of deposition over the entire 'box' this will not be directly comparable to the samples taken throughout the room. The CFD model, however, should allow for estimates of deposition to be determined at specific points within the room (i.e. at the positions of the samplers).

2.8.3 *Answers to regulatory questions*

While the data collected during this experiment does not in itself provide answers directly to the regulatory questions, the analysis of these data in comparison with the model predictions will provide important further insight for the two questions identified as being relevant to the task;

Q11: What are the (main) determinants of occupational and consumer exposure?

Q12: How should human and environmental exposure be assessed in practice?

Analysis of the data alone can be undertaken to determine whether any of the factors that were varied within the experiment (ventilation, material, source) have a significant impact on the concentrations measured, and subsequently whether these factors can be thought of as main determinants of exposure.

The data will be used to test the quantitative exposure models and so will enable estimation of the accuracy and uncertainty of the predicted concentrations. The accuracy can be evaluated for a few scenarios (varying emission pattern, ventilation rate and material) allowing for feedback on which situations the model works best and potentially identifying why the model may be underperforming in other scenarios.

The results of the model testing/validation will be combined, along with the outputs of other tasks being carried out within T3.4, to develop guidance for users of exposure models and tool. The guidance document will look to identify the applicability domain of each tool/model, what information is essential to obtain a sensible estimate of exposure, how reliable these estimates are likely to be. In addition recommendations will be made to model/tool developers to highlight the potential issues with their model/tool identified through the validation/testing process as well as any factors which they should take into account.

This work will help to promote confidence in the use of exposure models to carry out exposure assessment as the user will understand better which tool/model they should use for their specific needs and what the result obtained actually means for them.

2.8.4 *Provision of data for testing exposure models and assessment tools*

After having completed the tests of data consistence, the consortium will make the data available also to external partners for further evaluation. This way, a validated dataset will become available for assessing the different exposure models and assessment tools.

The conditions for data sharing will be specified at a later stage of the project.

A publication is under preparation that will provide a link to the data.

3 Deviations from the work plan

The DoW contained an error in the title of Deliverable 3.4. With agreement with the NANOREG Management Committee the title of D3.4 was update to "Improved data for the modelling of the exposure to MNM".

The experiment outlined here was not defined in the original description of work. On planning the scope of work within Task 3.4 at the outset of the project it was decided that data should be generated within the task that could be used to test/validate the models and/or investigate the determinants of exposure. This was originally envisaged to be done via a series of small-scale experiments in small testing chambers/lab settings, however it was agreed that it would be more beneficial to the task overall to concentrate efforts in undertaking this large-scale collaborative experiment.

4 Annex

2.10 Material Data Sheet for NM-203

Representative TEM image	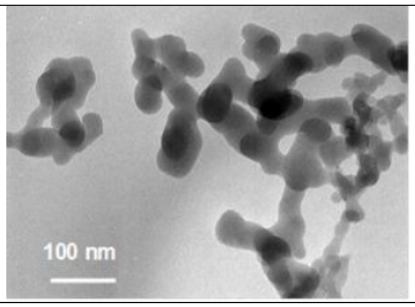
Main Phase	Synthetic Amorphous Silica (SAS)
Minor Impurity phases	Na_2SO_4, AlO(OH) (by XRD)
TEM primary particle size ECD [nm] (n=3)	24.7±17.7
TEM length of primary particle [nm]	NA
XRD size [nm]	not relevant
SAXS aggregate size [nm]	NA
DLS Zeta aggregate size [nm]	175±7
BET SSA [m^2] (n=1)	204
SAXS SSA [m^2] (n=1)	167±13
Major elements	Si, O
Minor elements/coatings (EDS) Na [wt%] Ca [wt%] Al [wt%] S [wt%]	Al, S ND ND 0.43 0.04
Organic coating [wt%]	-
Organic compounds	ND
IEP [pH]	2 to 4
Zeta-size and reactivity in 0.05% BSA water DLS Zeta-size BSA medium [nm] 24-hour dissolution pH reactivity dO_2 Reactivity	 127±2 SAS and Al-impurity partially soluble (-) +
Rotating Drum Dustiness Inhalable dustiness index [mg/kg] (n=3) Respirable dustiness index [mg/kg] (n=3)	 5800±1488 354±6
Vortex shaker dustiness Respirable dustiness index [mg/kg] (n=1)	 51000

[€] *data from n laboratories*